The rheological characterization of jetting fluids at high shear rates using a piezo axial vibrator.

Olov Rosén

Master of Science Thesis MMK 2014: 82 MDA 424

KTH Industrial Engineering and Management

Machine Design

SE-100 44 STOCKHOLM

Examensarbete MMK 2014: MF204X

KTH Industriell teknik och management

Rheologisk Karakteriseringen av jetting vätskor vid höga skjuvhastigheter.

Olov Rosén

Godkänt	Examinator	Handledare
	Jan Wikander	Mohammad Khodabakhshian Khansari
	Uppdragsgivare	Kontaktperson
	Gustaf Mårtensson	Olov Rosén

Sammanfattning

Detta examensarbete omfattar konstruktion, tillverkning och testning av en ny typ av reometer, med målet att karakterisera vätskor vid höga skjuvhastigheter. Projektet genomfördes vid Micronic Mydata AB och förknippas med de jetprinting lösningar företaget erbjuder för produktion av elektronik. En litteraturstudie genomfördes inom reologi innan förverkligandet av prototypen. Denna typ av rheometer (*Piezo Axial Vibrator*) bygger på excitationen av ett vätskeprov med hjälp av ett piezoelementet, samtidigt som den resulterande deformationen mäts. Förbättringar görs på den föreslagna designen och en grundlig analys med avseende på strukturell-resonans sker innan tillverkningen av prototypen.

Elektronik anpassad för denna applikation är utvecklad tillsammans med ett grafiskt gränssnitt för att styra processen. Med spännings och skjuvnings-komponenterna från vibrationen studeras fas och amplitudsvar för ett brett frekvensområde. Denna enhet är testad med Newtonska vätskor av olika viskositeter, samt viskoelastiska fluider med skjuvförtunnande egenskaper. Resultatet jämförs med vad som kan erhållas med hjälp av konventionella reometrar. Slutsatsen är att den framtagna rheometern visar stor potential i att karakterisera komplexa fluider. Stor repeterbarhet och noggrannhet uppnås tillsammans med förmågan att anpassa anordningen för mätningar på ett brett utbud av vätskor.

Slutligen diskuteras eventuellt framtida arbete som involverar omarbetning av elektroniken samt bearbetning av mätdata till en mer användbar representation.

KTH Industrial Engineering and Management

Master of Science Thesis MMK 2008: MF204X

The rheological characterization of jetting fluids at high shear rates using a piezo axial vibrator.

Olov Rosén

Approved	Examiner	Supervisor
	Jan Wikander	Mohammad Khodabakhshian Khansari
	Commissioner	Contact person
	Gustaf Mårtensson	Olov Rosén

Abstract

This thesis covers the design, manufacturing and testing of a *Piezo Axial Vibrator* type rheometer, with the goal of characterizing jetting fluids at high shear rates. The project was carried out at Micronic Mydata AB and is associated with jet printing for the production of electronics. A literature study is conducted on the field of rheology prior to the realization of the prototype. The working principle of the PAV is based on the deformation of a fluid sample using a piezo element, while simultaneously measuring the response. Improvements are made on this proposed design and a thorough analysis with respect to structural resonance is conducted before manufacturing the device.

Electronics tailored for this application is developed along with a GUI for controlling the measurements and sensors. By using the stress and strain components of the vibration, the phase and amplitude response is studied for a broad frequency range. This device is tested with Newtonian fluids of different viscosities, as well as viscoelastic fluids with shear thinning properties. The result is compared to what can be obtained using conventional rheometers. It is concluded that the developed rheometer shows great potential in characterizing complex fluids. Great repeatability and accuracy is achieved along with the ability to adapt the device for measurements on a wide variety of fluids.

Finally, possible future work is described involving rework of the electronics as well as the processing of the measured data into a more useful representation.

FOREWORD

I would like express my gratitude towards all who have helped me in my thesis. Without this assistance this project would not have been near as successful. I would like to thank Gustaf Mårtensson for allowing me to do this fun and exciting project and for his guidance throughout the process. I appreciate the resources and equipment that has been put at my disposal that made it all possible.

Finally, I would like to thank family and friends for their support in times of adversity.

Olov Rosén

Stockholm, April 2014

NOMENCLATURE

Here are the Notations and Abbreviations that are used in this Master thesis.

Notations

Symbol	*Description*
F	*Force (N)*
m	*Mass (Kg)*
k	*Spring constant*
d	*dampening*
E	Young´s modulus (Pa)
r	Radius (m)
t	Thickness (m)
σ	Shear stress (Pa)
ε	Normal stress(Pa)
γ	Shear strain
$\dot{\gamma}$	Shear strain rate (s^{-1})
ω	Angular velocity (Rad/s)
f	frequency (Hz)
t	Time (s)
V	Voltage (V)
I	Current (A)
R	Resistance (Ω)
P	Power (W)
X	Reactance (Ω)
C	Capacitance(f)
L	Inductance(H)
T	Temperature (°C)

Abbreviations

CAD	Computer Aided Design
RTD	Resistive temperature detector
DMM	Digital Multimeter
FEA	Finite element analysis
SGS	Strain gauge Sensor
PAV	Piezo axial Vibrator
EMI	Electromagnetic interference
PCB	Printed Circuit Board
CMRR	Common Mode rejection Ratio
SMPS	Switch Mode Power Supply
MOSFET	Metal Oxide Semiconductor Field effect transistor
PCI	Peripheral Component Interconnect
IC	Integrated Circuit
GRSE	Ground Reference Single Ended
GUI	Graphic User Interface
SMT	Surface Mount Technology

TABLE OF CONTENTS

1 INTRODUCTION

This chapter describes the background, problem description and the goal of this project. Basic theory in the field of rheology and piezoelectricity is covered. This chapter also explains conventional rheometers and their limitations. This thesis took place at Micronic Mydata's premises in Täby, Sweden.

1.1 Background

Micronic Mydata AB is a Swedish company engaged in the development, manufacture and marketing of production solutions to the electronics industry. The company's main business area includes pattern generators and surface mount technology equipment, the latter including pick and place equipment and jet printing solutions. This thesis is associated with the jet printing branch.

Jet printing is a technique for applying solder paste to *printed circuit boards* and offers an alternative to conventional screen printing using stencils. The working principle is the same as for an inkjet printer; functional material is deposited on a substrate using a piezoelectric element in a print head. Combining this with an xy-table, the solder paste is applied to the board in a software controlled manner, unlike screen printing where the stencils have to be made specifically for each design. This offers a flexible solution and drastically shortens lead-times.

In addition to solder paste, other types of materials can be applied as well, such as adhesives for fixating components. These materials differ in their rheological properties, i.e. their flowing properties, and the jetting parameters of the machine must be set accordingly. There is an interest in measuring the rheological properties both for the material provider and for those developing the technology. Making these measurements correctly can tell whether a material is jetable or not and also help optimize jetting results.

The materials of interest are complex fluids with both viscous and elastic components and act shear thinning, i.e. their shear viscosity decreases as they are subjected to increasing shear rate. Solder paste is basically metal powder solder suspended in solder flux. Flux is a cleaning agent, but also allows the paste to flow smoothly. If the properties of a certain suspension are known, it is expected that if the particles are interchanged while maintaining the same size and proportions, the properties will remain the same. This would give the possibility to make accurate predictions on the properties of a suspension if the flux is known properly. This would minimize the needed rheological measurements.

This thesis covers the design and manufacturing of a rheometer prototype. A device that measures these rheological or flowing properties. A literature study is done in the field prior to the practical work and the work is in part inspired by an earlier project (Kirchenmann, 2003). The work is limited to the designing, building and testing of the prototype. The post-processing of the data is omitted in this thesis.

1.2 Rheology

Rheology is the study of the flow of fluids having both viscous and elastic properties when subjected to deformation. Many of the fluids of interest for industrial applications possess complex microstructures such as polymers, suspensions and colloids. Elasticity in a material means the ability to store and release energy and this leads to materials that can have a memory effect. The way a material responds to stress can depend on recent deformation. This is associated with a certain stress relaxation time. For time intervals longer than the relaxation time, the material has forgotten this stress and thus behaves in a viscous manner. Depending on the time scale of the flow, the fluid behaves differently. The *Deborah number* is defined as the ratio between a materials relaxation time,τ, and the time of the flow, *t*, and describes this phenomenon.

$$De = \frac{\tau}{t} \tag{1}$$

For a high *Deborah number*, the fluid shows elastic properties, while for a low number it shows viscous properties. This can be related to the jetting process, where the fluid undergoes many different flows of different timescales. It is worth noting that a material will behave like a solid if the timescale is short enough.

For purely viscous materials, so-called Newtonian fluids the rate at which the material is sheared is simply proportional to the shear stress according to Newton's viscosity law (equation 2). The proportionality constant, μ, is called the *shear viscosity* and can be thought of as the resistance to flow. Higher viscosity means more resistance to flow.

$$\sigma = \mu\dot{\gamma} \tag{2}$$

Solids do not deform continuously and the shear stress, σ, is proportional to the shear strain γ, according to Hooke's law, where *E* is the shear modulus.

$$\sigma = E\gamma \tag{3}$$

One way to describe a viscoelastic fluid is to combine the contribution from equation 2 and 3 in a mechanical model. A simple model is the Maxwell model, which consists of a spring and dashpot connected in series shown in figure 1.

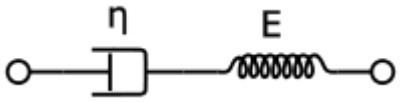

Figure 1. A Maxwell model consisting of a spring and a dashpot.

In this model, the strain rate, $\dot{\gamma}$, is the sum of the viscous and elastic strain rates

$$\dot{\gamma} = \dot{\gamma}_E + \dot{\gamma}_V. \tag{4}$$

Differentiating Hooke's law and inserting in previous equation yields

$$\dot{\gamma} = \frac{\dot{\sigma}}{E} + \frac{\sigma}{\mu}. \tag{5}$$

The time constant of this system is the ratio

$$\tau = \mu/E. \tag{6}$$

such that

$$\sigma + \tau\dot{\sigma} = \mu\dot{\gamma}. \tag{7}$$

In the case of a sinusoidal input signal, this can be expressed as the complex relation

$$E(i\omega)\gamma_0^* e^{i\omega t} = \left(i\omega + \frac{1}{\tau}\right)\sigma_0^* e^{i\omega t}. \tag{8}$$

We introduce the *complex shear modulus* where

$$\sigma = G^*\gamma, \tag{9}$$

where

$$G^* = G' + iG'', \tag{10}$$

where G' is the *storage modulus* and G'' is the *loss modulus.*

Combining equation 9 with equation 8 gives

$$G^* = \frac{i\omega\tau E}{1+i\omega\tau}. \tag{11}$$

By multiplying with the complex conjugate of the denominator one gets

$$G^* = \frac{E\omega^2\tau^2}{1+\omega^2\tau^2} + i\frac{E\omega\tau}{1+\omega^2\tau^2}. \tag{12}$$

Using waveform representation, the stress can be expressed as

$$\sigma = \frac{E\omega\tau\gamma_0}{(1+\omega^2\tau^2)}(\omega\tau\cos(\omega t) - \sin(\omega t)). \tag{13}$$

The stress has thus two components. The *storage modulus G'* is the part where stress and strain are in phase and is found by setting $\sin(\omega t)$ to zero. The *loss modulus G''* is the part where stress and strain are out of phase and is found by setting $\cos(\omega t)$ to zero.

$$G' = \frac{E\tau^2\omega^2}{(1+\omega^2\tau^2)} \tag{14}$$

$$G'' = \frac{E\tau\omega}{(1+\omega^2\tau^2)} \tag{15}$$

It is customary to express the rheological properties using these components.

1.3 Conventional rheometers

As of today, these materials are measured using rotational rheometers. These types of devices consist of two surfaces with a small amount of sample in between shown in figure 2. By fixating one plate and rotating the other with a certain frequency, while measuring the applied momentum, the viscosity can easily be calculated together with equations of the flow. Intuitively, it is easy to understand: having a thicker or more viscous sample will increase the momentum needed to rotate the plate.

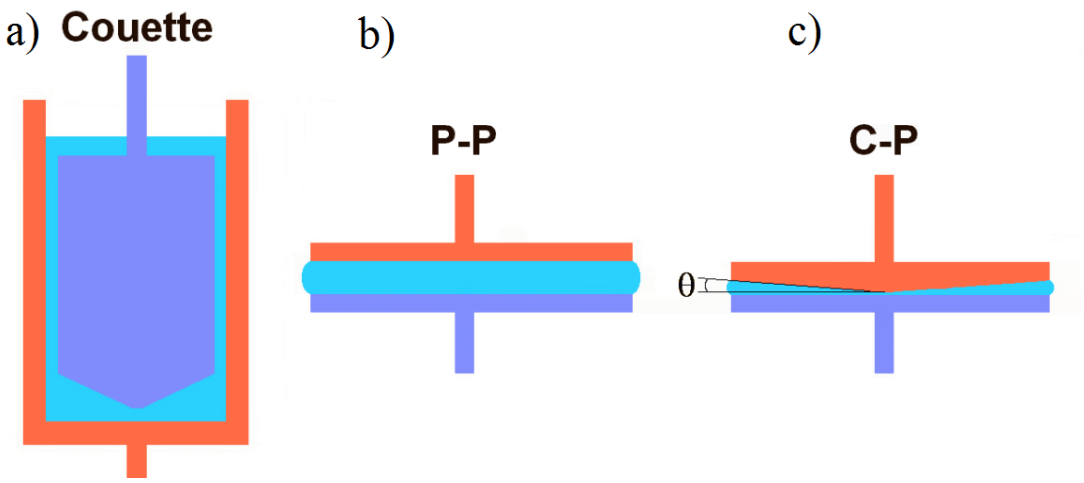

Figure 2. A cross section of different rotational rheometers: a) a Couette, b) a plate–plate, c) a cone-plate design. The sample is shown in blue. The fixated part is shown in dark blue and the rotating part in orange.

1.4 Oscillatory measurements

The previously explained technique is limited to measuring the shear viscosity of the sample. If the elastic properties are to be found one must consort to oscillatory measurements. This concept could be explained using figure 3. If an oscillatory shear stress is applied to a sample using an actuator, this results in a strain. For a Hookean solid, i.e. a material following equation 3, the strain is completely in phase with stress. For a viscous sample, however, the stress is proportional to the strain rate (equation 2). The strain rate is just the time derivative of the strain and is thus 90 degrees ahead. For a completely viscous material, the measured strain would therefore lag 90 degrees behind the stress

For a viscoelastic material, one need to look at the phase difference δ between the stress and strain in order to see how viscous or elastic it is. More phase lag means a more viscous material while less means more elastic. The numerical values of viscosity and elasticity can be found using the amplitude values of the stress and strain. With a larger viscosity, the response is smaller since the material is not as easily sheared, while the phase difference remains the same.

This type of test can be done using rotational rheometers by applying a sinusoidal rotation speed.

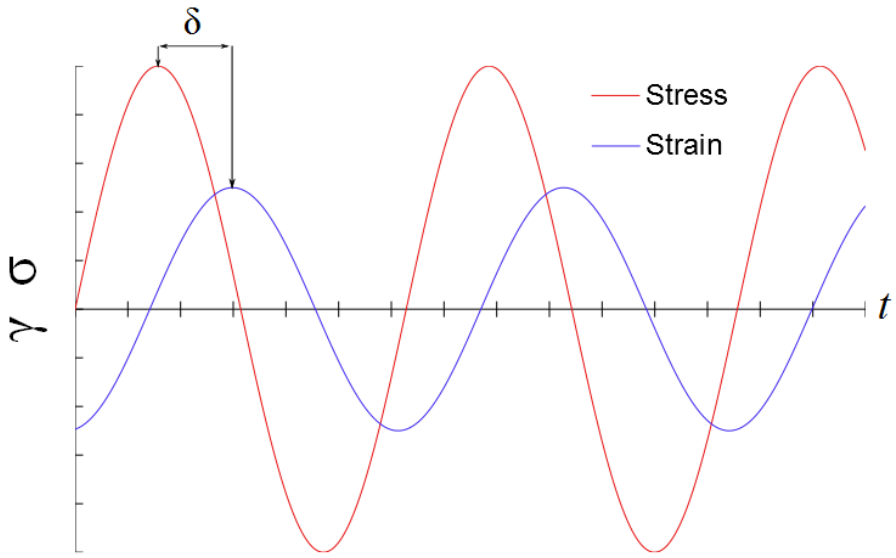

Figure 3. Working principle of oscillatory measurements: The phase difference tells how viscous or elastic the material is.

The actual stress and strain that are measured are not those of the fluid and one must consort to constitutive equations and mechanical relations to calculate the shear modulus. Effort should be made in order to measure stress and strain components that can be easily converted to that of the fluid.

1.5 Limitations in rotational rheometry

In the process of jetting, the material undergoes a wide range of shear rates. The material is fed into the print head using a screw pump. Once in place, the material is ejected onto the substrate with an impulse from a piezo element. The timespan of this ejection is in the microsecond range and thus resulting in a very high shear rate. Because of the shear thinning properties of the materials, there is a different viscosity associated with every shear rate and because the jetting process involves many stages with different shear rates, one would have to measure the viscosity for all of these shear rates to predict the jetting behavior.

Rotational rheometry is limited with respect to achievable shear rate. At high rotation speeds wall slip starts occurring and this causes the calculations to fail. This makes it impossible to measure the rheological properties at the high shear rates occurring during jetting. The purpose of this thesis is to investigate an experimental type of rheometer that is capable of achieving a much higher shear rate.

One could resort to capillary rheometers, where the material is extruded through a die while pressure and piston speed are being monitored. This type of rheometer is both difficult to set up and uses a lot of sample material. This is undesirable since many materials are expensive.

Another drawback of using rotational rheometers is that this technique is destructive with respect to the material structure. The material is continuously sheared during measurement, actively changing structural properties, such as volume fraction homogeneity. This may result in properties that make the material unjetable being actively removed by measurement.

Rotational rheometers depicted in figure 2 are usually powered by stepper motors and although oscillatory measurements can be carried out, their moving parts are associated with high inertia. In order to increase the bandwidth, one must minimize inertia of moving parts, as well as consort to better and faster means of creating this displacement. Piezo elements are an excellent alternative and are used in the design covered in this thesis.

1.6 Axial oscillatory vibrations

One possible way of conducting this oscillatory shear flow is by vibrating a sample in between two circular plates in their axial direction, depicted in figure 4. When the sample is contracted, a squeeze flow occurs in the radial direction. Similarly, when the sample is extended, the flow is reversed. If one of the plates is subjected to a sinusoidal force, a sinusoidal deformation occurs and one obtains the situation in figure 3. In this way, the problem with wall slip is removed since the flow close to the plates is zero.

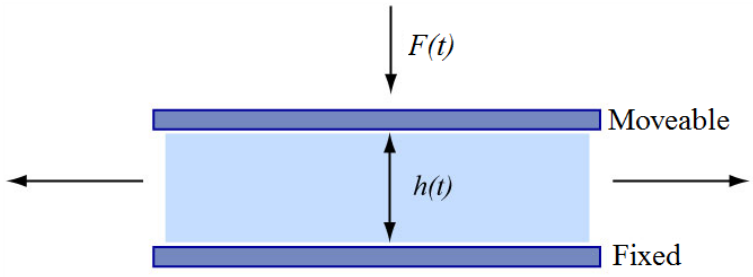

Figure 4.The resulting squeeze flow when two plates are compressed.

By analyzing this flow, one could relate the complex shear modulus to the mechanical domain. The complex spring constant that the sample corresponds to is calculated by Ludwig Kirchenmann (2003) and yields this equation

$$K^* = \frac{3\pi}{2} \cdot R \cdot \left(\frac{R}{d}\right)^3 \cdot \frac{G^*}{1 + \frac{\rho\omega^2 d^2}{10G^*} + \dots} \tag{16}$$

where R is the radius of the plate, d is the thickness of the sample, ρ is the density of the sample and ω is the angular velocity of the oscillating motion. This is derived under the assumption of incompressible flow, constant sample area and neglecting pressure effect on the edges. This equation describes the behavior when vibrating a sample in between two plates and will be used as a basis in the design.

This type of oscillatory motion was used in a design by Kirchenmann (2003) called a *Piezo axial vibrator*. The rheometer built in this thesis also incorporates axial vibrations in a similar but improved design adapted for measurements on jetting fluids.

1.7 Design by Kirschenmann

The rheometer design proposed by Ludwid Kirschenmann (2003) works as follows: A sample is placed in between two plates, where the upper plate is fixed and the lower plate is connected to a square copper tube. Piezo elements are glued onto the sides of the tube and two are used as actuators and two are used as sensors. With this design, along with constitutive equations, such as equation 16, Kirschenmann obtained some interesting result for polymer solutions.

This design had several issues, however. The amplitude of the displacement was in the nanometer range resulting in a tiny input and output signal resulting in a bad signal to noise ratio. This was overcome partly by the use of a lock in amplifier capable of detecting a signal obscured by noise thousands of times larger.

The signals that were used for the calculation of amplitude and phase were the drive signal and response signal of the piezo elements. Although these signals are proportional to both stress and strain, contributions from other sources are present. This gives signals that are highly dependent of the system itself. In order to obtain a reliable result the device needs to be thoroughly calibrated. Resonance peaks in the measurement range also posed problems. Low resonance frequencies gave a very limited measurement range and the low amplitude limited the shear rate.

The goal of this thesis is to produce a new design that implements axial oscillatory vibrations using piezo elements adapted for particle solutions, such as solder paste with the goal of achieving high shear rates.

1.8 Piezoelectric effect

Certain crystal solids have the ability to accumulate electric charge in response to mechanical stress. This is known as the *piezoelectric effect* and was discover by Pierre Curie in the mineral quartz. The crystalline structure of the ceramic lead titanate, which has this property, is shown in figure 5. This ionic compound, consisting of an oxide of lead, titanium and zirconium is a so-called *ferromagnetic material*. Below a certain temperature called the *Curie temperature*, the crystal structure exhibits a dipole moment. The smaller free moving anion, titanium or zirconium, creates a polarization by changing the symmetry of the crystal shown in figure 5. When an external electric field is applied across the polarization axis, a deformation occurs, proportional to the strength of the field.

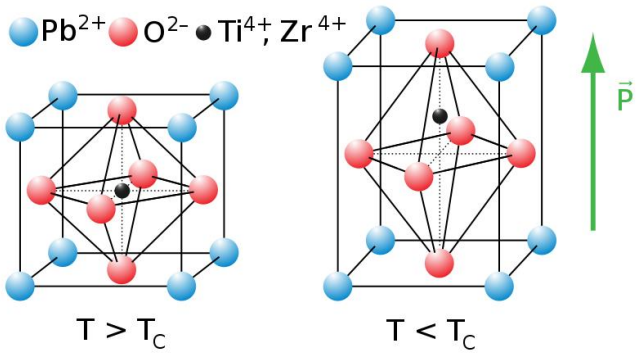

Figure 5. Crystalline structure of lead titanate illustrating the piezoelectric effect below the Curie temperature.

The structures align in local areas or domains and although each crystal element exhibits this piezoelectric effect the net effect in the material is zero. By poling the material, shown in figure 6, the domains rearrange, giving the material anisotropic properties. When applying an electric field in the poling direction, the entire material now deforms.

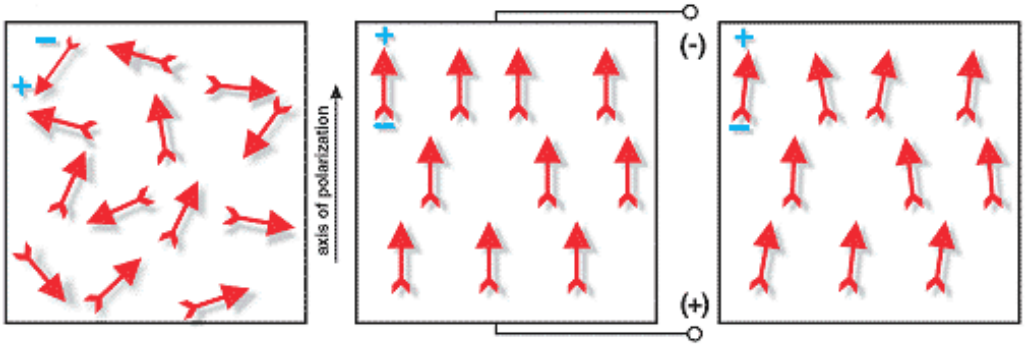

Figure 6. Poling of a piezo material. To the left) the domains are oriented randomly giving isotropic properties. In the middle) an external field orients the domains. To the right) the polarization remains after the field is removed.

The piezoelectric effect can be described by

$$D = eE + d^d\sigma, \tag{17}$$

$$\varepsilon = d^cE + s\sigma\ , \tag{18}$$

where D is the dielectrical displacement, e is the electrical permittivity, s is the elastic compliance, d^d and d^c are piezoelectric coefficients. When a piezoelectric material is expanding in the direction of the polarization, a perpendicular contraction occurs, called *Possion's effect*.

1.9 Piezo stack actuator

The deformation in a piezoelectric material follows equation 17 and 18. To achieve a large strain, the applied electric field needs to be large. To obtain the displacement, the strain is simply multiplied by the thickness of the material. The electric field is created by applying a voltage to electrodes at the surfaces of the material. If the distance between the electrodes increases, the electric field decreases. One would need a very large operating voltage to obtain a considerable displacement this way. A solution to this is to stack multiple thin piezo discs with alternating polarization separated by electrodes. In this way, the electric field is unaffected by the thickness of the actuator and large displacements can be achieved by using many layers shown in figure 7. The displacement of a piezo stack with n layers can be estimated by

$$\Delta L \approx d_{33} \cdot n \cdot U \tag{19}$$

where n is the number of layers and U is the driving voltage.

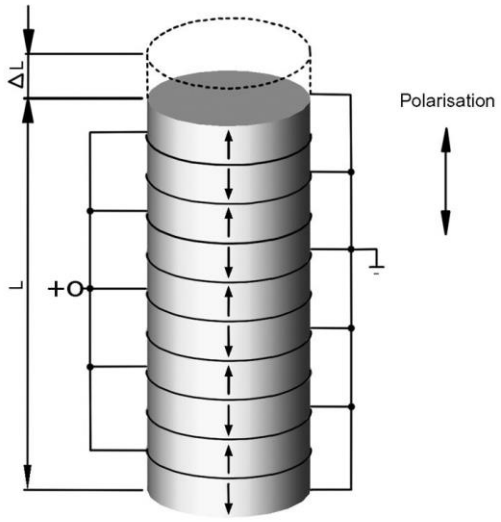

Figure 7. Working principle of a piezo stack with 10 layers

A piezo stack solution is chosen for this project so that a large displacement can be created in a very compact design. A compact design is preferred since it minimizes the risk of resonance. The design by Kirschenmann (2003) utilized the Possion contraction and gave a very non-rigid structure, resulting in low resonance frequencies in addition to a very small displacement.

1.10 Temperature dependence of viscosity

Viscosity is a highly temperature-dependent property and tends to decrease as temperature increases. A consequence of this is that a measurement of viscosity is only valid in a small range around a specific temperature. Therefore, it is of great importance to measure the viscosity at multiple temperatures or at a desired working temperature. The temperature also needs to be kept within a reasonably small range throughout the measurement for the value to be correct.

There are many equations relating temperature and viscosity and are valid for different materials and temperatures. One fairly accurate model is the Arrhenius equation proposed by Svante Arrhenius in 1889, which states

$$\eta(T) = Ae^{\left(\frac{E}{RT}\right)} \tag{20}$$

where A is the pre-exponential factor, R is the universal gas constant, T is the temperature and E is the activation energy for viscous flow. E is the minimum energy needed for a flow to occur and also determines the temperature sensitivity of the fluid.

To calculate the viscosity at a specific temperature, both A and E needs to be determined. If the ratio between the viscosity of a reference temperature and the viscosity of the measurement temperature is derived, the dependence of A is removed.

$$\frac{\eta(\mathrm{T})}{\eta(\mathrm{T}_{ref})} = e^{\left(\frac{E}{RT} - \frac{E}{RT_{ref}}\right)} \tag{21}$$

By plotting this ratio as a percentage change versus the deviation in temperature between the measurement temperature and reference temperature, figure 8 is obtained. The numerical value of the activation energy *E* for different solder pastes is taken from Nguty and Ekere (2000). This activational energy is derived using three different flux agents for three different shear rates. One can conclude that a deviation of two degrees centigrade from a reference temperature of 25 degrees would change the viscosity as much as 10%. This change in viscosity is not arbitrary, however. As temperature increases the viscosity decreases, making it possible to compensate for this effect if the temperature is monitored properly.

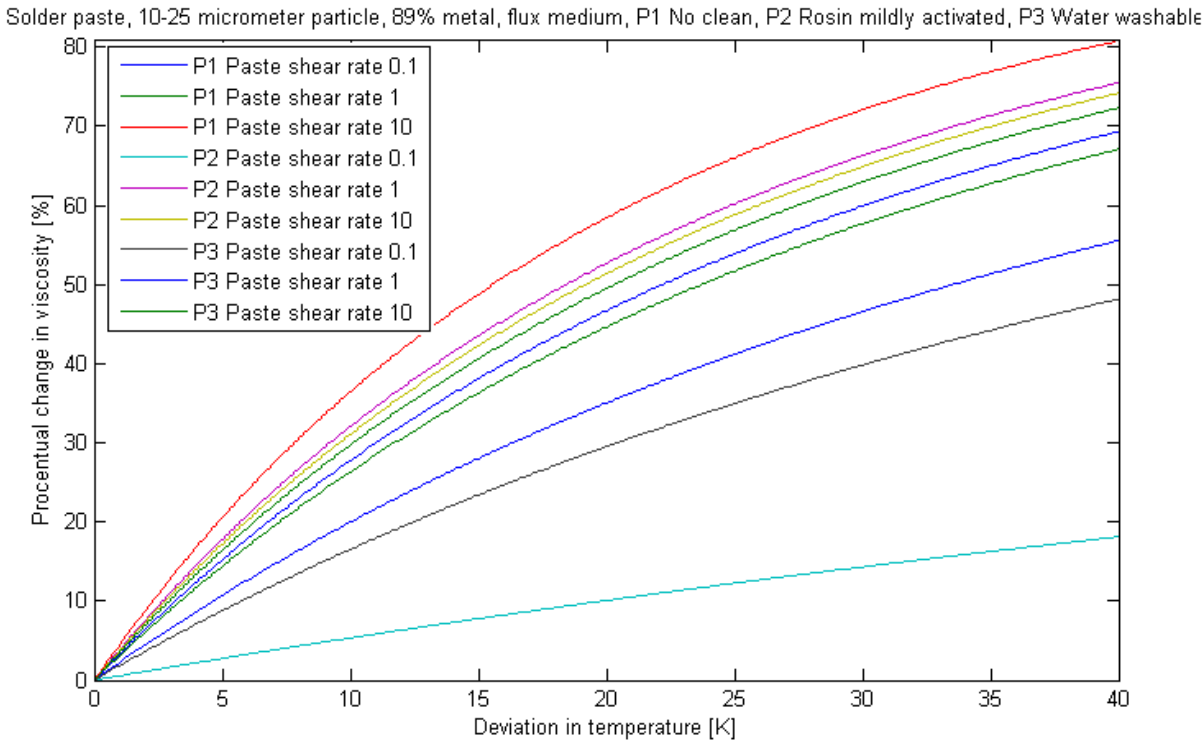

Figure 8.Temperature dependence of viscosity for different solder pastes.

1.11 Requirements

Early in this project, the requirements that the rheometer should fulfill are stated to ensure that the goal is properly defined and the right system is built. An excerpt of this list follows.

- The rheometer shall measure viscosities ranging from 1 mPas to 1 kPas.

For comparison this would mean the viscosity of water ranging up to the viscosity of thick peanut butter.

- The rheometer shall conduct oscillatory measurements from 100 Hz up to 10 kHz in frequency.
- The temperature at which measurement are conducted shall be 20-35 degrees centigrade with a deviation during measurement of less than 0, 5 degrees.

A full list can be seen in the appendix.

2 MECHANICAL DESIGN

This chapter describes the design process for the mechanical components and the analysis behind the decisions taken. It covers the simulations that have been made prior to the realization of the system.

2.1 Initial design

The design consists of an upper and lower plate separated by a spacer with the sample in between. The lower plate works as membrane and a piezo stack placed underneath allows the sample area to oscillate. The upper plate remains fixed resulting in an oscillating squeeze flow of the sample. Both the upper and the lower plate have trenches next to the sample area, as can be seen in figure 9. The gap size outside the sample area is orders of magnitude larger than on the inside and thus the forces outside this area can be neglected. This can be realized by changing the parameter *d* in equation 16. This is done so that the area of the sample can be considered constant in the post processing of the data.

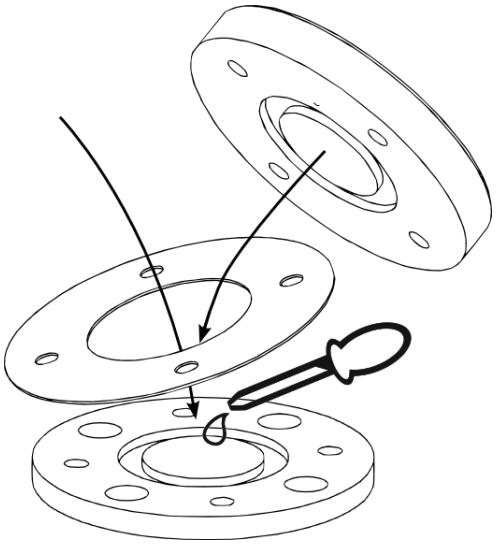

Figure 9. The upper and lower plate with their defined sample areas and trenches separated by a sheet metal spacer.

The piezo stack is made of a rather brittle material and cannot accommodate tensile loads. When the piezo stack is subjected to high dynamic loads the forces needed to accelerate the stack can rip it apart. This can be solved by adding a preload to the piezo stack in such a way that the pressure is always compressive throughout the load cycle.

The preloading mechanism consists of a slider connected to the bottom of the piezo stack and can be seen in figure 10. The magnitude of the preloading force can be adjusted with a setscrew located in the bottom lid and the output of the piezo stack is read simultaneously in order to obtain the correct pressure.

The piezo stack cannot accommodate momentum and two screws hold the slider in place, but can move in a slot in the axial direction. The lower plate is fixed to the body with four screws to

allow that once that the preload has been set, it can be sealed and this procedure does not have to be redone.

The initial design can be seen in an exploded view in figure 10. To calculate the rheological properties of a sample, both the stress and strain need to be measured. It is however impractical to measure the stress and strain of the fluid itself and it is the stress and strain of the actuator that is measured. The force of the piezo stack is measured with a piezo sensor that is initially attached to the lower plate. The strain is measured with a strain gauge attached to the side of the piezo stack. Using constitutive equations, one can relate the stress and strain of the piezo stack to that of the fluid.

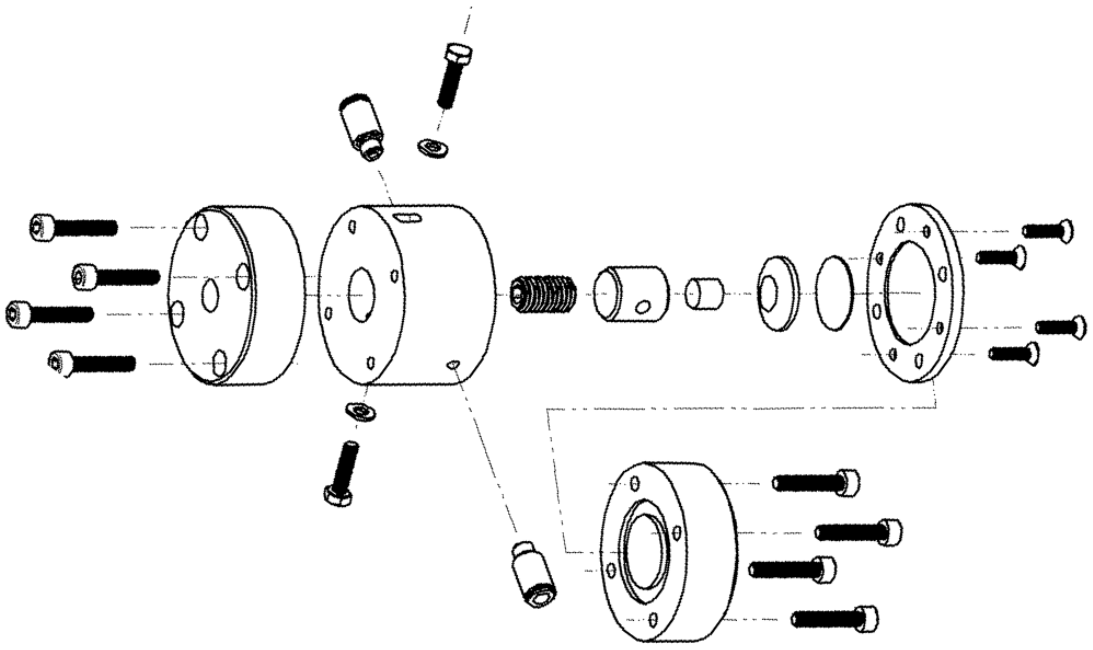

Figure 10. An exploded view of the mechanical parts of the first design.

According to equation 16, the force that the fluid exerts on the plate is dependent on both the gap size and the viscosity of the sample. By changing the gap size, this force changes, as well. The system itself is designed to exert a certain force on the plate and by changing the gap size, different viscosities can be measured using the same system. A smaller gap size is suitable for lower viscosities while a larger is more suitable for higher viscosities.

This system is designed to measure the properties of solder pastes with particle sizes less than 25 µm. The gap size between the plates must be big enough to remove the effects of particle interactions. The considered gap sizes are: 200 µm, 400 µm and 600 µm, which is at least 8 times larger than the biggest particle. Sheet metal spacers are made with these thicknesses. The use of equation 16 requires that the diameter of the sample is much larger than the size of the gap. A diameter of 25 mm is chosen for this design.

The loading procedure is a critical step. To load the device, the upper plate is removed along with its four screws and the sample is applied. If the sample does not cover the entire sample area, or if air bubbles are in the sample, the result will be incorrect. The volume required to con-

duct the measurements can easily be calculated as the sample area times the thickness of the spacer. The correct volume is applied preferably using a pipette.

To further increase redundancy, multiple measurements should be considered for each fluid. It is then easy to discard any faulty measurements due to improper loading and the reliability of the results increase.

2.2 Resonance

In the requirements, it is stated that the rheometer shall conduct oscillatory measurements in the range: 100-10000 Hz. The measurement technique is based on the relationship between the applied force and the resulting strain and how these are affected by the sample. The strain is not only affected by the sample, however. The dynamics of the mechanical parts play a role, as well. For the unloaded system, i.e. when no sample is present, the ideal case would be that the strain is unaffected by the frequency at which the load is applied, but this is not the case. The mechanical system itself has a tendency to sustain oscillations at certain frequencies, a phenomenon known as *resonance*. Vibrational energy can be stored at these frequencies, although some is lost each cycle in what is called *damping*.

Due to the low damping in a steel structure, the resonance frequencies are approximately the same as the natural frequencies of the system. One way of finding the resonance frequencies analytically is to set up an equivalent mass-spring system, as seen in figure 11. In this system, with two degrees of freedom, the lower plate is subject to a time varying load, simulating the force from the piezo stack. This is a rather crude depiction since only two point masses are allowed moving in one direction, but this can be used in estimating the dimensions of the system, as well as in the post processing of the measurement data.

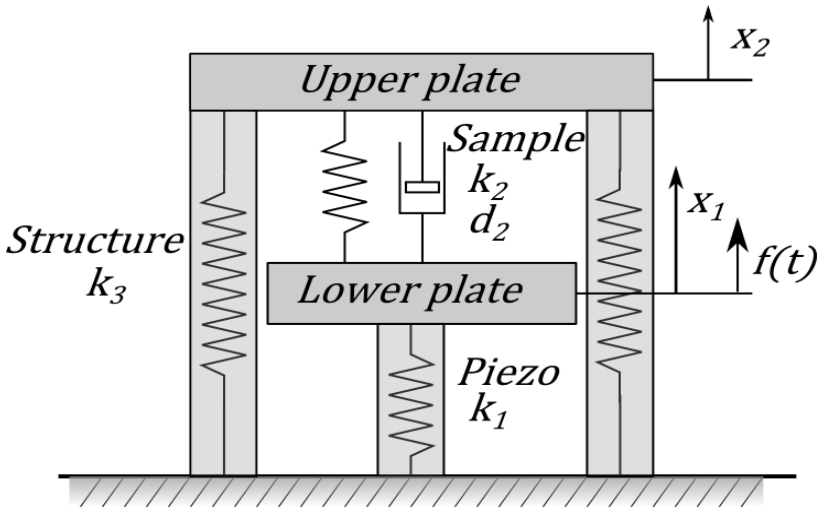

Figure 11. Mechanical equivalent of the rheometer

A force balance on both masses gives

$$m_1\ddot{x}_1 = f(t) + x_1(k_1 + k_2) - k_2x_2 + d_2(\dot{x}_1 - \dot{x}_2) \quad (22)$$

$$m_2\ddot{x}_2 = x_1(k_1 + k_2) - k_2x_2 + d_2(\dot{x}_1 - \dot{x}_2) \quad (23)$$

Using matrix notation one obtains

$$\begin{bmatrix} m_1 & 0 \\ 0 & m_2 \end{bmatrix}\begin{bmatrix} \ddot{x}_1 \\ \ddot{x}_2 \end{bmatrix} = \begin{bmatrix} f(t) \\ 0 \end{bmatrix} + \begin{bmatrix} k_1 + k_2 & -k_2 \\ -k_2 & k_1 + k_2 \end{bmatrix}\begin{bmatrix} x_1 \\ x_2 \end{bmatrix} + \begin{bmatrix} d_2 & -d_2 \\ -d_2 & d_2 \end{bmatrix}\begin{bmatrix} \dot{x}_1 \\ \dot{x}_2 \end{bmatrix} \tag{24}$$

This can be expressed as

$$\boldsymbol{M}\frac{d^2\boldsymbol{x}}{dt^2} = \boldsymbol{F} + \boldsymbol{K}\boldsymbol{x} + \boldsymbol{D}\frac{d\boldsymbol{x}}{dt} \tag{25}$$

This is a second order linear differential equation. Finding the natural frequencies is done by finding the eigenvalues of

$$\boldsymbol{K}\boldsymbol{X} = \lambda \boldsymbol{M}\boldsymbol{X} \tag{26}$$

This has two eigenvalues corresponding to two resonance modes: one in which both masses oscillate in phase and one where they are out of phase. Modeling this part correctly is a necessity if the complex shear modulus is to be calculated, since the system dynamics greatly affects the measurements.

2.3 Modal analysis

Once the preliminary design is made, a modal analysis is conducted to find its resonance frequencies. This modal analysis incorporates a *finite element method,* to find an approximate solution to the differential equations describing the motion of the body. The model is discretized into nodes and meshes, thus reducing the degrees of freedom. This makes it possible to find approximate values for many mechanical properties, such as resonance frequencies. This is initially done with the built-in simulation tool in Solid Edge, but is later done in the more powerful simulation environment ANSYS. All material is set to steel with a Young's modulus of 200 GPa, except for the piezo stack with the lower stiffness of 58 GPa. The modal analysis in conducted under the assumption that the structure is rigidly fixated at its bottom face. This removes all resonances associated with the free movement along the axes and shows only those that contain some elastic deformation.

The first six resonance frequencies are shown in table 1. The two first modes correspond to the bending of the structure along the two horizontal directions. The third is the torsional mode. The fourth is the elongation of the structure. Resonance frequencies 5 and 6 are the second order bending of the structure including a stationary point in its waveform. It is not until mode 10 at 27 kHz that the resonance of the lower plate occurs. Some of these resonance modes are more likely to be excited than others, for instance; the elongation mode could easily be excited, for its motion is in the same direction as that of the piezo stack. For the torsional mode however, no actuator is putting energy in that direction, which should give it low amplitude. It can be concluded that three resonance frequencies are within the measurement range.

Table 1.The resonance frequencies for the first six modes of the rheometer structure.

Mode:	Frequencies [Hz]
1 ”Bending” x	5122,2
2 ”Bending” y	5127,7
3 Torsional	9533,1
4 Elongation	15018
5 2nd order ”bending”	16929
6 2nd order ”bending”	16976

2.4 Harmonic response analysis

In addition to the modal analysis, a harmonic response analysis is made in order to see how the system responds to the applied load and to which extent the different resonance modes are being excited. The force from the piezo stack is simulated as a sinusoidal force with amplitude of a 1000 N and frequencies up to 20 kHz are studied. The deformation of the lower plate is measured at the face in contact with the sample and its frequency response is shown in figure 12. All components are assumed rigidly connected and the bottom face is fixated. However, there is a problem with this assumption. Simulating the load from the piezo stack as a force does not resemble its physical behavior. The stack itself is stiff and does not deform easily. It takes a significantly larger force to obtain the desired deformation in this depiction than it would take when the piezo element actually deforms due to the piezo electric effect. With that said, it is the shape of these amplitude response curves that is of interest rather than their numerical values. They are also used in observing this amplitude changes when changing the mechanical design.

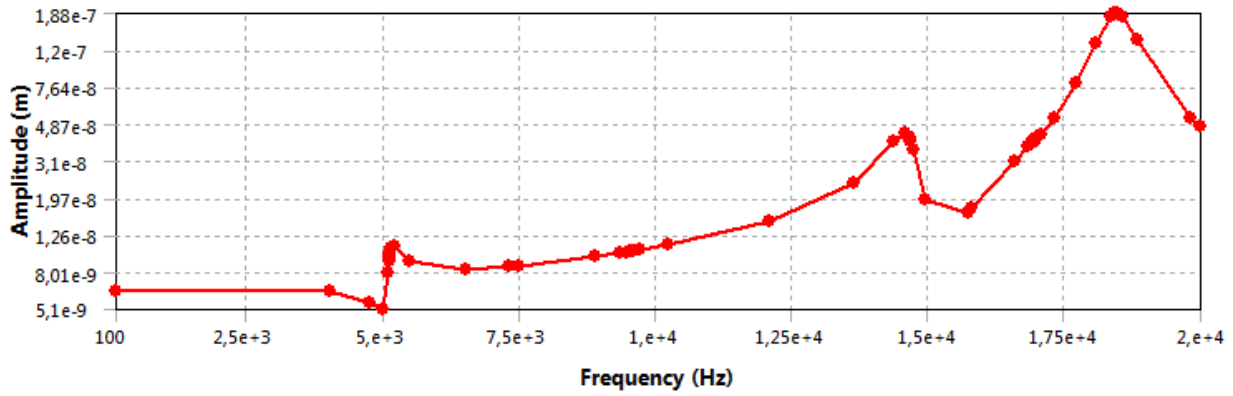

Figure 12. Frequency response of the displacement in the lower plate when the system is driven by a sinusoidal load.

It can be seen in figure 12 that the resonance mode 1 and 2 affect the movement of the lower plate. As expected, the torsional mode has no impact on this response since its deformation is close to zero in the axial direction. The order of this amplitude is low.

2.5 Change of design

To overcome the resonance frequency in the measurement range due to the bending of the structure, a small change is implemented in the design. As a guideline: the lowest resonance frequency in a clamped rod follows equation 27, where a is the thickness and L is the length. By making the design shorter and wider this frequency increases. The width is increased by 10 mm and the length is shortened by 10 mm. The frequencies of mode 1 and 2 are increased to 6896,6 Hz by this change in design and can be seen in table 2.

$$f_1 = 0.162 \frac{a}{L^2} \sqrt{\frac{E}{\rho}}. \tag{27}$$

Table 2.The resonance frequencies for the first six modes after a change in the design.

Mode	Frequencies Hz
1 ”Bending” x	6896,6
2 ”Bending” y	6920,6
3 Torsional	10876
4 Elongation	17458
5 2nd order ”bending”	19654
6 2nd order ”bending”	19790

To increase the amplitude of the response, the weight of the moving parts is decreased. This is done by moving the sensor to the bottom of the piezo stack, as well as making the lower plate thinner. This increases the response by a factor 200.

The frequency response is derived as described earlier and is shown in figure 13 for the new design. One can see that the amplitude for the first resonances has dramatically decreased and moved up in frequency and the only main peak is the elongation mode found at 17 kHz.

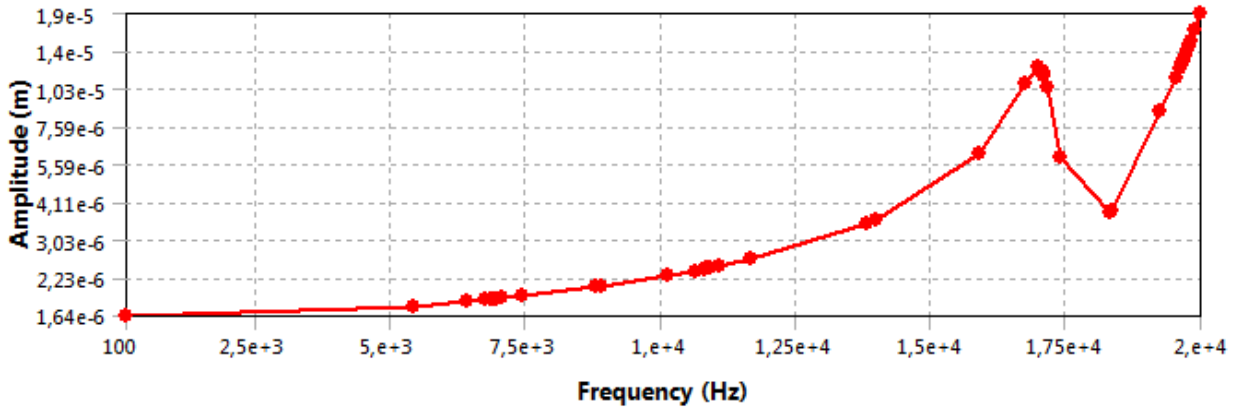

Figure 13. The frequency response after a change in design.

2.6 Final design

The final design can be seen in an exploded view in figure 14. In order to minimize the weigh while distributing the force of the piezo stack, a cone shaped area is made at the bottom of the lower plate. As stated earlier, the lower plate works as a membrane and it is designed in such a way that the majority of the deformation occurs outside the sample area where the thickness is small. The bending of the sample area is undesirable since its conflicts with the assumptions made in the equations regarding the squeeze flow. Some bending is unavoidable, but it is decreased once the sample is in place. Another drawback of this membrane design is that a lot of the force goes into deforming the lower plate rather than deforming the actual sample. The benefits of this design are greater still. High dimensional tolerances along with a compact design with high resonance frequencies make this concept favorable. This solution also promotes robustness and ease of use.

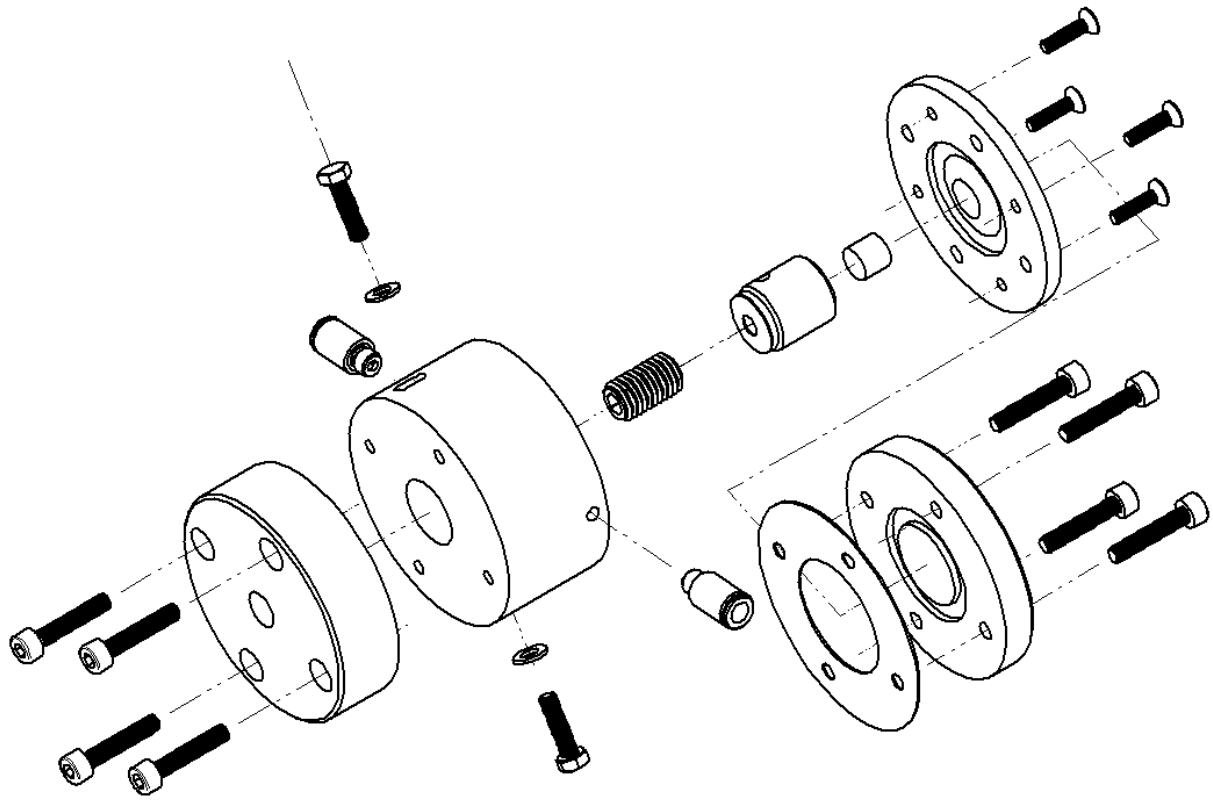

Figure 14. An exploded view, showing the final design of the rheometer.

2.7 Drafts

Drafts are created from the derived model of the rheometer. There are five parts in the design that needs to be lathed. The spacers are thin profiles and need to be either water cut or laser cut. The material chosen for the body and bottom lid is: *s235jrg*, a common structural steel, and for the upper and lower plate a stainless steel: *1.4301* is chosen. Stainless steel is picked for the parts that are in contact with the sample to prevent corrosion and to improve the long term use.

The surfaces of the lower and upper plate need to be fine so that viscous forces do not arise from the roughness of the surface. A value of the maximum surface roughness for these surfaces is specified as *Ra 0.8*. The definition of *Ra* is the arithmetic average of the absolute values of the profiles height deviation along the specified surface.

Another reason for specifying this low surface roughness is that the surfaces become very flat. If the thickness tolerance of the spacer is fine, the parallelism between the upper and lower sample area becomes high. This is very desirable according to equation 16, where small deviations in the gap size greatly affect the result.

Ra 0.8 is generally not achievable with a lathing operation and another surface grinding operation needs to be performed.

The general tolerance for the mechanics is stated as *ISO 2768-mk*. Hole and shaft tolerances are specified for the hole in which the slider is. These are set to obtain an easy running clearance fit.

Standard socket cap M5 screw with coarse threading is used in this design. For the lower plate, countersunk flathead screws are used. This is so that spacer can be put on top of this screw.

These mechanical components are processed by the company MERX and the finished parts are shown in figure 15.

Figure 15. The finished mechanical parts and fasteners.

2.8 Choosing piezo element

The oscillatory displacement is created using a piezo stack. The force that is needed is estimated by equation 16, as well as a static analysis using the simulation software ANSYS. By analyzing the lower plate, one can extract the force needed to achieve a certain displacement in the sample area. In figure 16, the displacement is shown when a 500 N force is being applied at the bottom face. It can also be seen that the displacement in the middle of the sample area is much bigger than at the edges, as discussed earlier. The effect of this is much smaller in the dynamic case however, where stress and strain are not in phase.

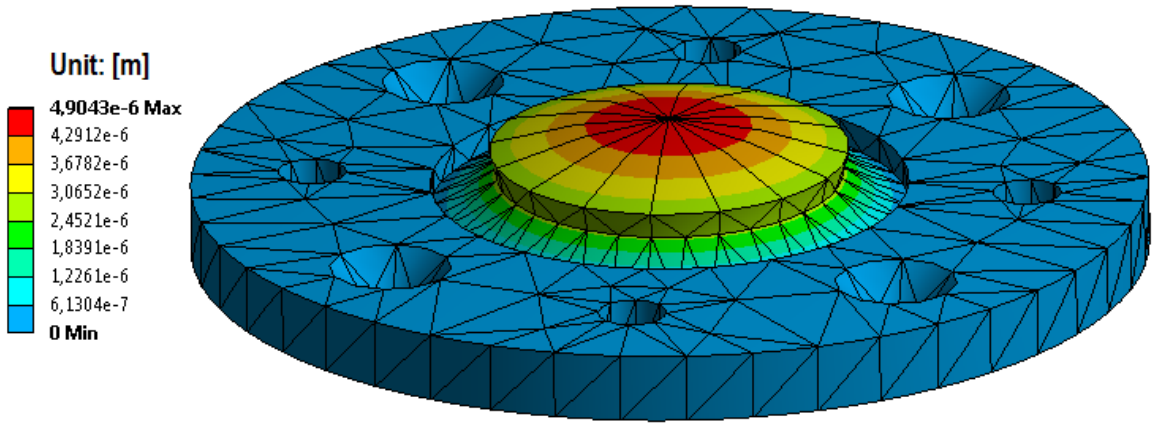

Figure 16. The displacement in the lower plate when subjected to a 500 N force. The deformation is exaggerated.

Equation 16 together with a nominal displacement of 1 µm provides the force needed for the squeezing of the sample and by using some reasonable values for the physical parameters, one obtains a decent estimate of the order of magnitude of this force. It is of great importance to find a piezo stack with the right force and displacement so that its electrical capacitance is minimized, thus reducing the difficulty in designing the driver later on. A piezo stack solution from the manufacturer Physik Instrumente is purchased for this application with a maximum displacement of 5 µm and a blocking force of 1200 N.

2.9 Force sensor

To measure the force of the piezo stack, a piezo disc is implemented as sensor. The piezo sensor is placed under the piezo stack, shown in figure 17. The placement of the sensor has great importance even though the force is distributed throughout the structure. If the sensor is connected to a mass that is subjected to an acceleration, that mass acts as a seismic mass and the signal is proportional to its acceleration. If the sensor is placed on the same side as the actuator, it can be used to measure the dynamics of the system itself. This is done by simply conducting a measurement without a sample and documenting the response. With the capability of making measurements on the dynamics of the system, one can isolate the effects of the sample. This is highly desirable since the system dynamics greatly affect the response. One could have the sensor located at the sample surface of the upper plate. In this way, most of the dynamics of the system would disappear. This solution would however expose the sensitive piezo disc and be difficult to implement with the desired tolerances. It was decided to place the sensor according to figure 17.

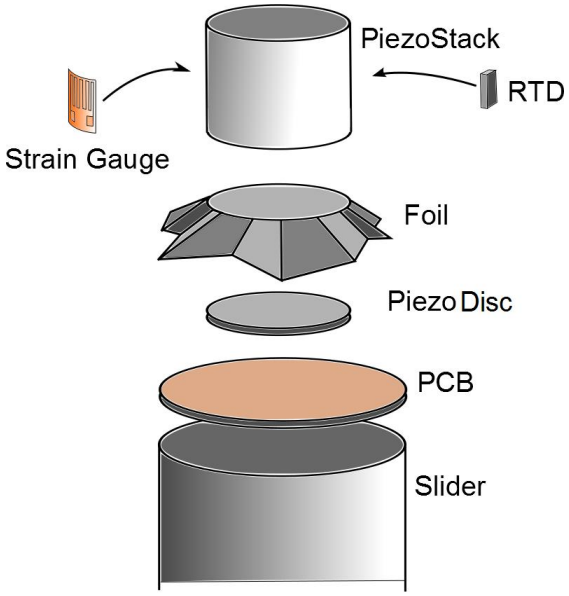

Figure 17 Sensor placements with respect to the piezo stack. A small printed circuit board connects to the Piezo disc and acts as strain relief for the cables

2.10 Electromagnetic interference

Driving the actuator demands high currents that in turn give rise to electromagnetic radiation in the cables. This radiation can induce a disturbing voltage in the surrounding cables, a phenomenon known as *electromagnetic interference*, or EMI. Since the amplitude of many of the measured signals is small, this application is highly sensitive to disturbances of this kind.

To prevent EMI, coaxial cables are used. These cables have an inner conductor surrounded by a woven copper shield with insulation in-between. The shield works as a *Faraday's cage* and effectively blocks electric fields.

To prevent the sensor from being affected by the electromagnetic radiation coming from the piezo stack, a thin copper foil is placed according to figure 17. This foil is connected to ground, preventing disturbances from reaching the force sensor.

2.11 Thermal analysis

A thermal analysis is conducted on the proposed design for two reasons: to see how the heat from the piezo stack affects the temperature of the sample and to estimate the temperature of the piezo stack and if cooling is required. If the sample is heated, its viscosity changes as shown in the introduction. According to Physik Instrumente, the dissipated power in the piezo stack, when driven by a sinusoidal signal, is approximately

$$P \approx \frac{\pi}{4} \tan\delta \, fCV_{pp}^2 \tag{28}$$

where tan δ is the *dielectric loss factor*, f is the frequency, C is the capacitance and V_{pp} is the peak to peak driving voltage. If the driving voltage is 600 V and the frequency is 10 kHz, this dissipated power is approximately 4 Watts. This may seem low but the small size of the piezo stack in combination with its poor thermal conducting properties may lead to high temperatures.

The *dielectric loss factor* tells how much of the electric power that is converted to heat within the piezo stack and is generally between 1-2%. It is, however, a function of the applied electric field and varies almost 50% over the entire voltage span. For the calculations of the dissipated power, the worst case value is used. The capacitance is in turn a function of the voltage and temperature and can vary as much as 200%, but for these calculations the value measured at room temperature is used.

2.12 Curie temperature

At a certain temperature, known as the *Curie temperature*, the piezo element begins to lose its polarization and the piezoelectric effect disappears. Different piezo materials have different Curie temperatures, but there is a tradeoff: a higher Curie temperatures results in a lower response to an applied voltage.

To avoid degradation of the material, the recommended operating temperature is usually half the Curie temperature. Physiks Instrumente offers a wide variety of materials for their piezo products. To allow high dynamics, which leads to high temperatures, a material with a Curie temperature of 350 °C is chosen.

2.13 Steady state thermal analysis

A steady state thermal analysis is conducted using ANSYS with the calculated dissipated power derived from equation 28. A few assumptions are made in this model. The rheometer is assumed rigidly connected to a base with infinite heat capacity and thus the bottom face is always kept at the ambient temperature. Heat is transferred through convection in the remaining outer surfaces with 10 W/mK. The thermal conductivity and heat capacity of steel is obtained from tabulated values, while for the piezo stack they are retrieved from the Physik Instrumente website. A thermal resistance between the surfaces connecting to the piezo stack is defined and estimated to 1000 W/m^2K. This is because ceramics generally have very poor conductivity at their surfaces. Radiation is neglected in this model.

The result from the thermal analysis can be seen in figure 18. Most of the structure is at ambient temperature, except for the piezo stack and the area close to it. There is a small temperature elevation in the lower plate however. This simulation is performed without the sample between the plates and in a real scenario this heat would be conducted by the sample. Still, there should be some concern of the sample being heated, as this changes its viscosity. The internal temperature of the piezo stack reaches 104 degrees centigrade. The operating temperature of the chosen piezo stack is 150 degrees, leaving a decent margin of safety. Viscous dissipation is neglected in this depiction, but it should not be considered negligible. This is difficult to model, however, and the temperature of the sample should be monitored.

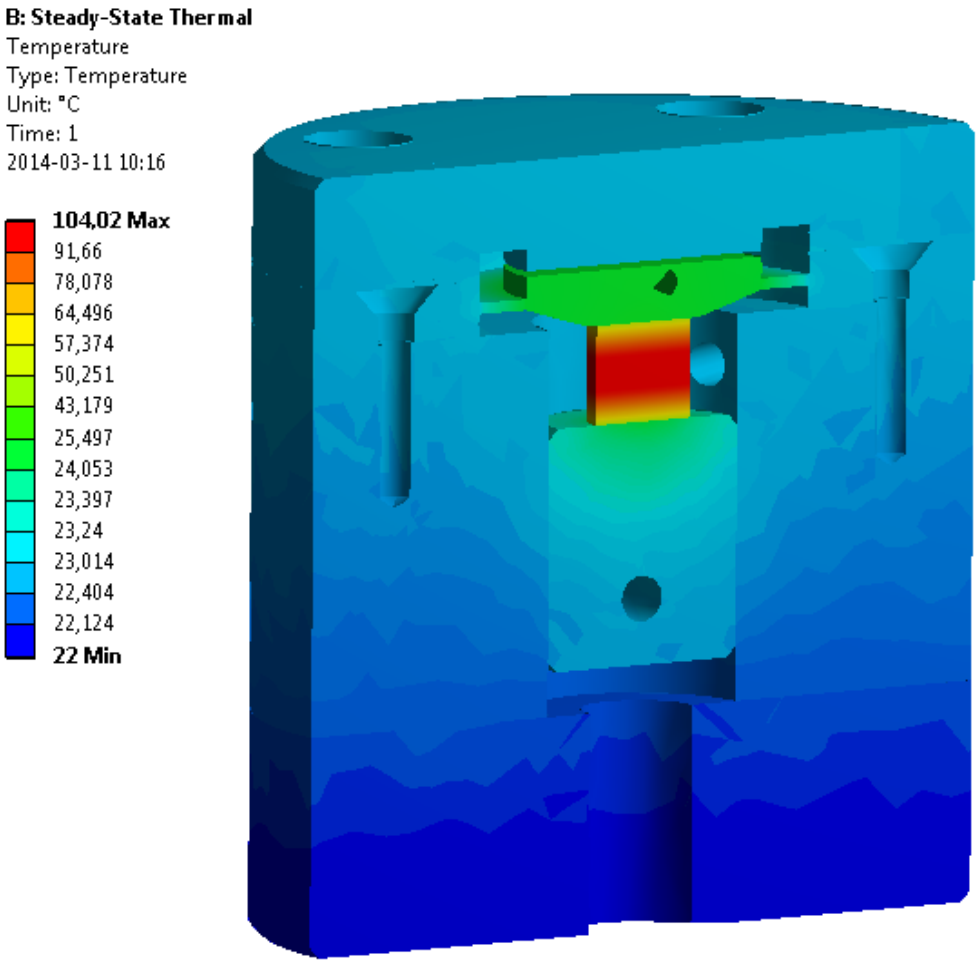

Figure 18. Temperature distribution in a cross-section of the design once thermal equilibrium is reached. The power of the heat generation is 4 W.

2.14 Transient thermal analysis

A transient thermal analysis is conducted to study the timeframe of this heating process. This is done to see if the measurements can be made before thermal equilibrium is reached, reducing the maximum temperature and allowing an increase in either voltage or frequency.

Using the same set-up as in the steady state model, the evolution of the temperature in the piezo stack is shown in figure 19. This process is fast and the rise time is about 30 seconds. The duration of a measurement is nearly the same, although the generated heat is noticeable only at high frequencies. During measurements a frequency sweep is made and the maximum frequency is only used a fraction of the time.

It is still decided that cooling should be implemented so that the driving voltage could be increased later on.

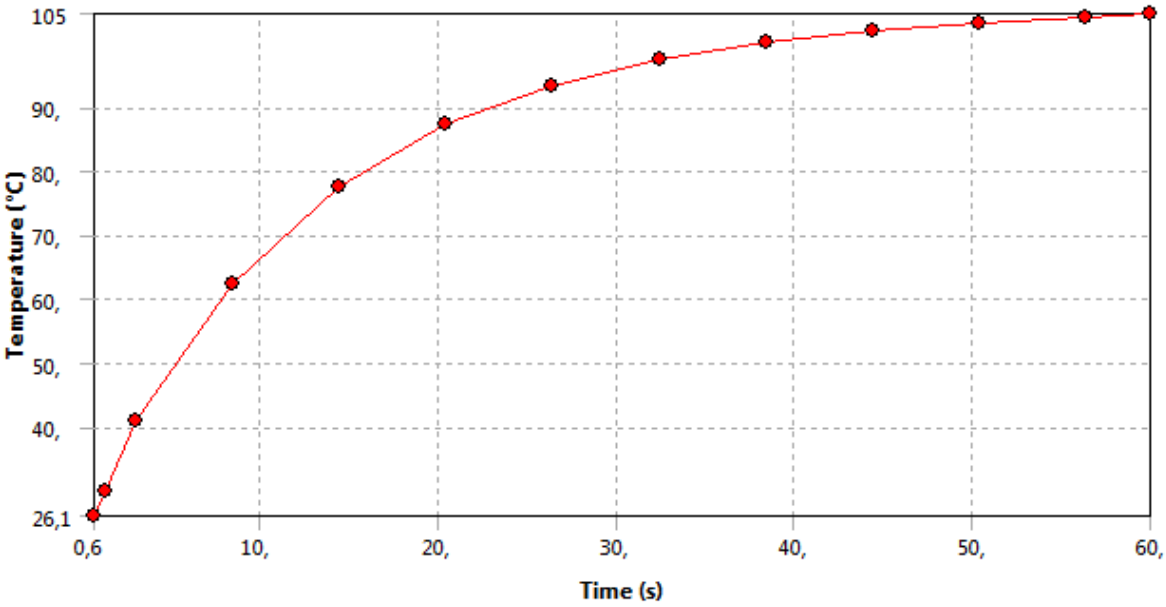

Figure 19.Evolution of the temperature in the piezo stack when dissipating 4 W.

2.15 Implemented cooling

Due to the heating of the piezo stack along with the temperature increase in the lower plate shown in figure 18, it is decided that cooling is needed. Cooling is implemented by ventilating the small chamber, where the piezo stack is located, with compressed air, shown in figure 20. A hole is drilled through the structure and an inlet is attached at one side and an outlet on the opposite side. A mechanical pressure regulator is used to control the flow.

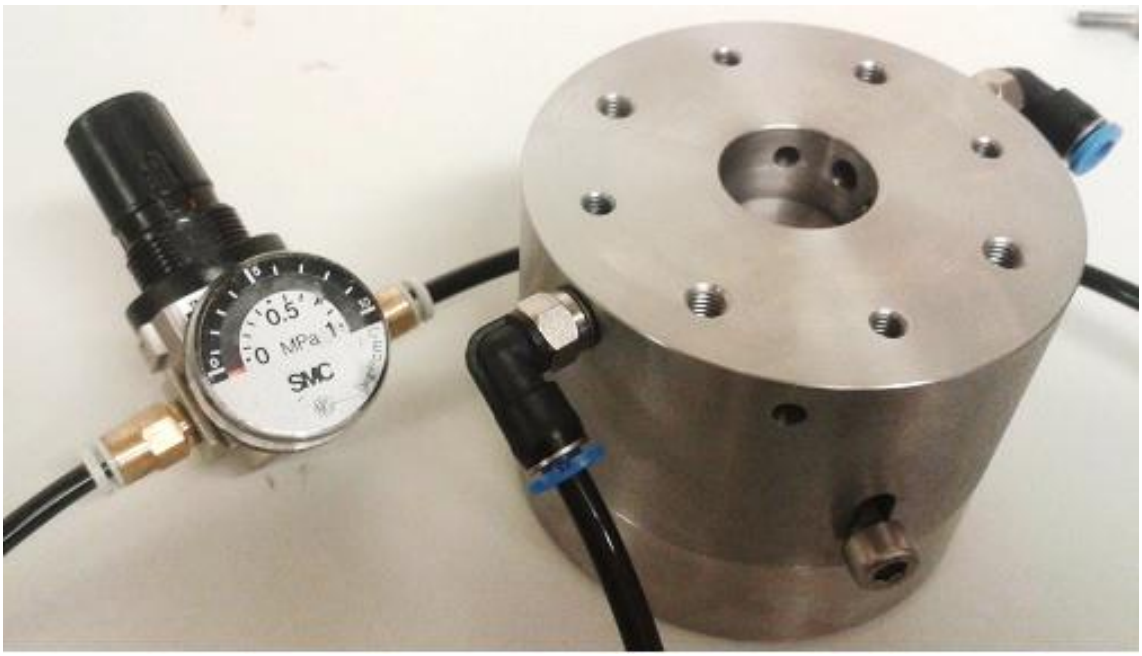

Figure 20. The air-cooled chamber and the mechanical pressure regulator.

2.16 Temperature sensors

For temperature measurements, resistive temperature detectors are used. This type of sensor detects temperature by changing its resistance in a linear way. The resistance is then measured using a *Digital Multimeter Device*. There are many sensors with different accuracy, tolerance and measuring range and for the piezo stack as well as the piezo driver, a sensor called *PT1000* is used.

For the measurements on the upper and lower plate, the smaller *PT100* sensor is used and a hole is drilled to fit the sensor as shown in figure 22. This sensor is delivered with three leads of which two are used for the sensor itself. The third is used to measure the resistance of the wires for compensation. The lead resistance measurements are made prior to the actual measurements and are later used in the calculations of the temperature.

Figure 21. Temperature sensors in the upper and lower plates.

2.17 Setting the piezo preload

According to the manufacturer, the recommended preload stress is 15 Mpa, or alternatively set in such a way that the stress is always compressive. To be able to set this preload correctly, the voltage corresponding to different stress values is examined. By doing so, the preload can be easily set by monitoring the voltage of the piezo stack until a certain value is reached. This relation is examined by making multiple measurements on the voltage, while the piezo stack is subjected to different forces. The force is generated by a crank and monitored with a load cell. To make sure that the voltage peak can be read easily, a capacitor is connected in parallel to the piezo stack. The result can be seen in figure 22 and shows a fairly linear relation.

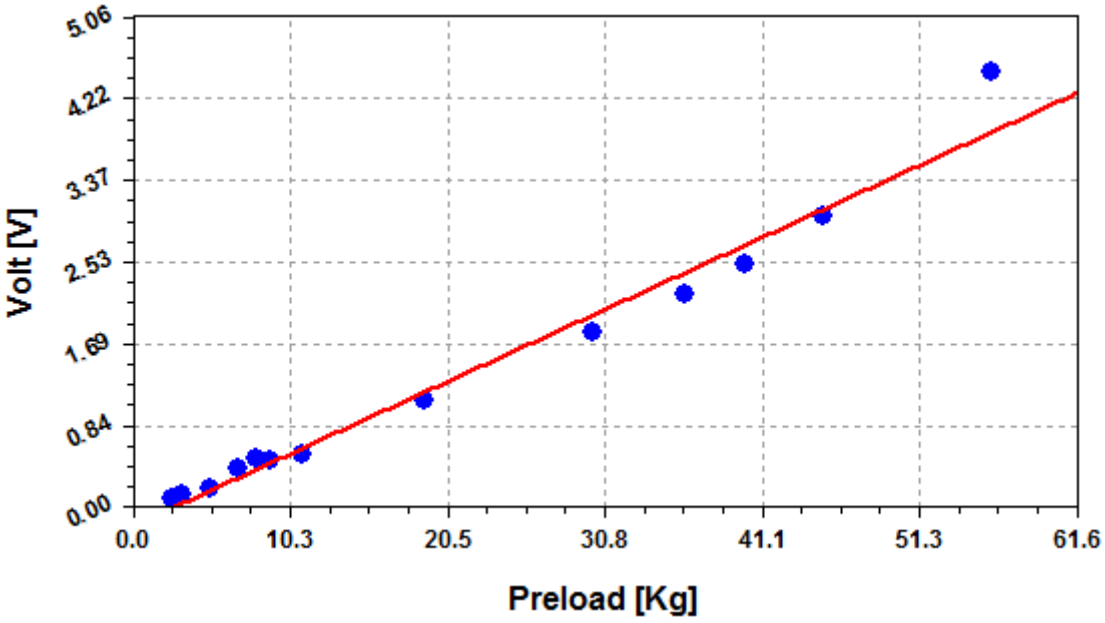

Figure 22.The preload force versus the voltage in the piezo stack. A linear curve fitting has been added.

2.18 Stress and fatigue

To make sure that the components can withstand the loads they are subjected to, the mechanical stress is calculated for the sinusoidal load case. The lower plate is particularly sensitive, since that component acts as a membrane and is exposed to large deformation. The stress can be seen in figure 23 and has a maximum value of 12 Mpa. This part is made of the stainless steel: 1.4301, which has minimum yield strength of 210 Mpa. The yield strength is defined as the minimum stress that gives a plasticity of 0.2%. Consequently, the safety margin against plasticity is large.

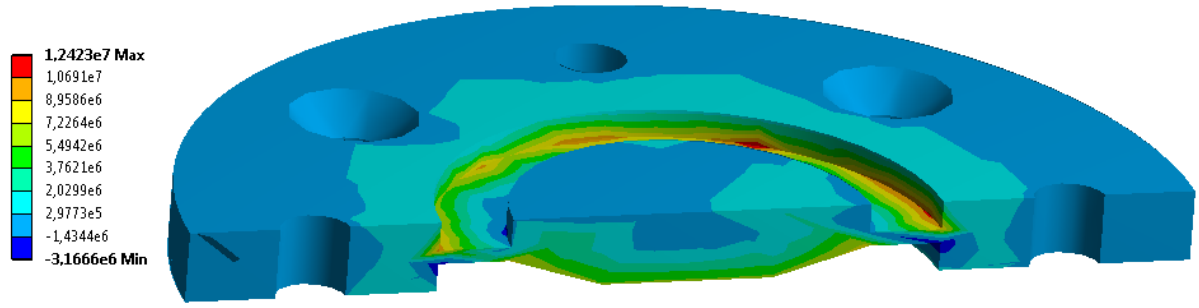

Figure 23.A cross section of the lower plate, showing the maximum stress during the load cycle.

Some materials can suffer from fatigue caused by oscillatory loads. Unless a certain fatigue limit is exceeded, this phenomenon does not occur for steel material. This limit is approximately half of the tensile strength, which in this case is at least 500 Mpa. It is concluded that the risk of fatigue is low.

2.19 Assembly

The force sensor is placed along with the piezo stack, according to figure 17, with a thin copper foil in between. The strain gauge and the temperature sensor are glued onto the piezo stack using a cyanoacrylate adhesive. For strain relief, the leads are soldered onto the PCB. Additional wires carry the signal through holes drilled for the cables. Outside the body, the wires are covered with a copper shield to prevent EMI and covered with shrinking tube for protection. BNC-type coaxial connectors are used for all cables, except for the temperature sensors, where Molex connectors are used, as shown in figure 24.

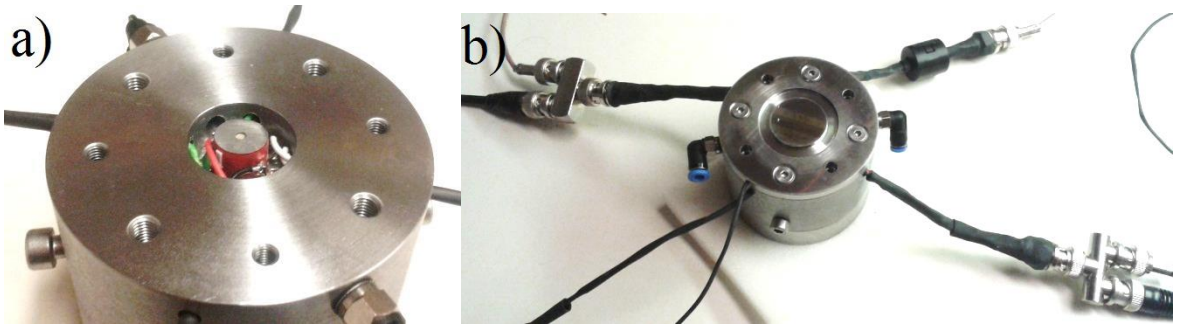

Figure 24. a) The piezo stack within its small chamber. b) The cabling.

3 ELECTRONICS

This chapter describes the design of the driving electronics, the sensors, filtering and disturbance rejection.

3.1 Driving Electronics

Creating a piezo driver with a power bandwidth of 10 kHz is no trivial task. A piezo stack is virtually a capacitor, with its displacement proportional to its charge. It is almost a purely capacitive load, which can generate stability issues. For static operations, it consumes almost no power, except for a leakage current of a few micro amperes. For dynamic operations, however, the piezo stack is charged and discharged for every load cycle. The power is dissipated as heat within the driver and is proportional to the driving frequency. There are regenerative drivers that are able to recover some of this so-called *reactive power*, but these are generally expensive and complicated.

Conventional piezo drivers used for positioning cannot achieve the required high bandwidth and the product range for these types of drivers is quite limited. A piezo driver tailored for the needs of this project is therefore constructed.

3.2 Power operational amplifiers

An effective way of driving a capacitive load is the use of power operational amplifiers. Fast, high power operational amplifiers can supply the needed voltage swing, while easily being controlled with a low voltage analogue signal.

An ideal operational amplifier is basically a voltage source which is proportional to an external voltage at its input. By implementing a feedback control, the electric potential at the input is increased and thus the output is amplified. This amplification is proportional to the ratio between the resistor at the output and the feedback resistor.

One particularly useful circuit using operational amplifiers is the differential configuration, shown in figure 25. With this configuration, the potential difference between V_1 and V_2 is amplified. In this way, unwanted signals that are common to both inputs are rejected, i.e. it possesses a high *common mode rejection ratio*.

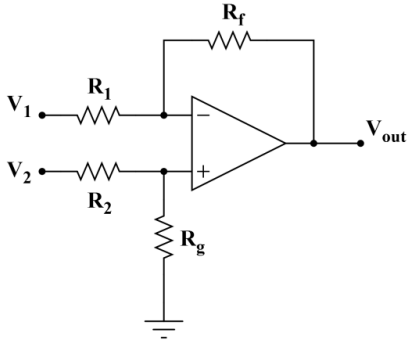

Figure 25. Differential configuration of an operational amplifier.

Using the same resistors for both inputs, i.e. R_1=R_2 and R_f=R_g, the output voltage can be calculated as follows

$$V_o = \frac{R_f}{R_1}(V_2 - V_1). \tag{29}$$

Apex Microtechnolgies supply fast, high power, high voltage operational amplifiers tailored for these applications. In order to select a proper operational amplifier, certain requirements need to be fulfilled. The speed at which the amplifier can change its output voltage is limited. This is defined as the maximum rate of change in voltage per unit time and is called *slew rate*. The needed *slew rate*, with a peak voltage of 150 V, can be calculated as follows

$$S.R = max\left(\frac{dV_{op}}{dt}\right) = 2\pi V_{op} f\ 10^{-6} = 9{,}4\ [V/\mu s]. \tag{30}$$

The maximum current that the amplifier must handle occurs at the highest frequency and is found by calculating the reactance

$$X_c = \frac{1}{2\pi f C} = 936\ \Omega. \tag{31}$$

Using *Ohm's law* the current is derived as

$$I = \frac{V_{op}}{X_c} = 160\ mA. \tag{32}$$

For the dissipated power within the operational amplifier, there are two contributing sources. The amplifier itself has a so-called *quiescent current*, when no load is applied, which is dissipated as heat. The other contribution is due to the load. For a simple resistive load, the power dissipation in the output transistor is simply

$$P = \frac{V^2}{R_{load}}. \tag{33}$$

For a reactive load, however, the dissipated power is given by the complex relation

$$\boldsymbol{S} = \boldsymbol{UI}. \tag{34}$$

With the power P, being the real part of the complex power $\boldsymbol{S}$ and depending on the phase between $\boldsymbol{U}$ and $\boldsymbol{I}$**.** A simplified formula provided by Apex Microtechnologies is

$$P_{DOUT} = \frac{4V_s^2}{2\pi X_c} = 15\ \text{W}. \tag{35}$$

A low cost amplifier that fulfills these requirements is PA78. With the calculated maximum dissipated power, a heat sink must be used. The temperature of the junction must be kept below 150 °C. From the junction, the temperature is conducted to the case with a certain thermal resistance. The case in turn, needs to be kept below 85 °C according to the datasheet. With no heat sink, the junction-to-air thermal resistance is stated to be 25 ºC/W. Based on this value, a heat sink must be used. A large heat sink is chosen to provide a safety margin.

3.3 Switch mode power supply

The PA78 can be delivered on PCB together with a *switch mode power supply,* capable of outputting 350 V, with a user-controlled switching frequency. This is favorable since all high voltage components would be integrated in one unit, thus protecting the operator.

The working principle of this type of boost converter can be explained by figure 26. When the switch is closed, current flows through the inductor, thus storing energy in the inductor. When the switch is open, the current is forced to flow through the diode instead. This new circuit has greater impedance and lowers the current. High voltages are induced within the inductor when this happens to prevent this change in current, according to *Faraday's law*. By switching with a high frequency, the output voltage can be much greater than the input voltage. The switch is a MOSFET controlled by an IC. The switching frequency governing the output voltage, is set by an external resistor. A potentiometer is used and the user can regulate the voltage freely, ranging from 50 to 350 Volts.

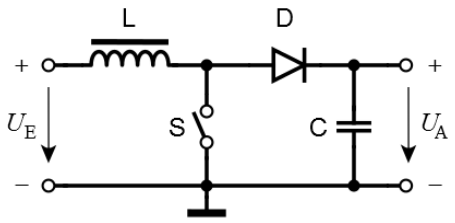

Figure 26. Working principle of a SMPS.

These types of power supplies give rise to disturbances due to their switching. Both ripples in the output voltage and EMI from the inductor are common.

3.4 Transient suppression

An *RC-snubber* seen in figure 27, is implemented to reduce the voltage spikes that occur in the inductor due to the switching. An alternative route for the current that reduces the rapid rise in voltage is provided.

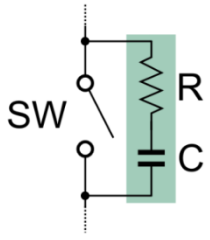

Figure 27. Working principle of a RC-snubber.

Bypass capacitors are connected to the boosted voltage, to reduce disturbances in the output stage. Two types of capacitors are used; a fast ceramic capacitor to reduce high frequency transients and a slower electrolytic one with higher capacitance for low frequencies. A fuse is added to protect the hardware in case of failure. The circuit diagram of the driver, created using Multisim, is shown in figure 28.

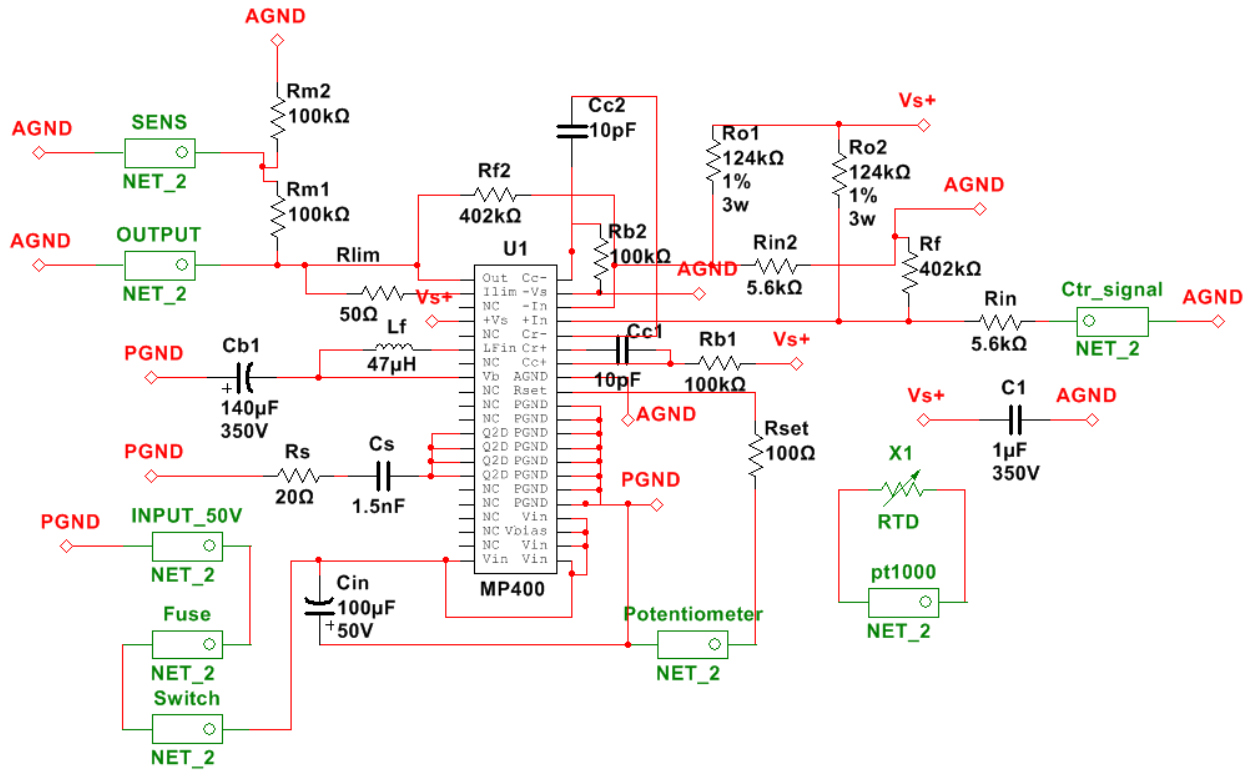

Figure 28.A circuit diagram of the piezo driver.

3.5 Electronic assembly

The proposed circuit design is soldered on a prototype PCB board and is enclosed in an aluminum casing, shown in figure 29. Holes are drilled and panel mount connectors are used.

In order to adapt the voltage levels to that of the acceptable levels of the DAQ-card and DMM, a voltage division is used. In this linear circuit, the output voltage can be set as a fraction of the input voltage. With appropriate resistors, the level is decreased by a factor of 10.

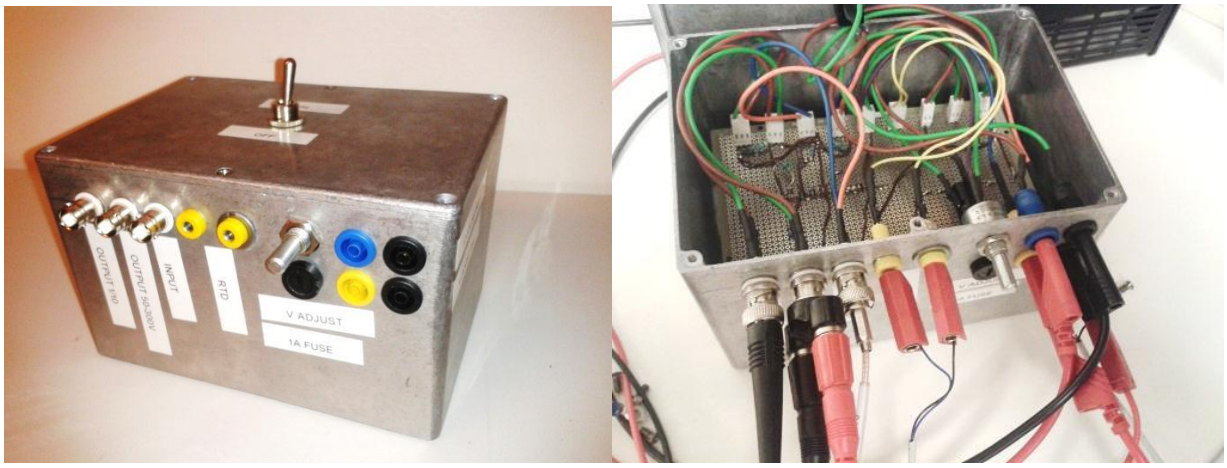

Figure 29. The protective enclosure of the driver and its interior.

3.6 Strain gauge

A strain gauge sensor is implemented and attached to the piezo stack to measure the deformation. A strain gauge consists of a thin metallic foil with a certain pattern, fixed to an insulating and flexible backing. Once the foil is subjected to a strain, the dimensions of the pattern changes as do the resistance of the leads. By measuring this change in resistance, the strain that caused it can be determined. The pattern can be made sensitive to deformation in certain directions, as shown in figure 30.

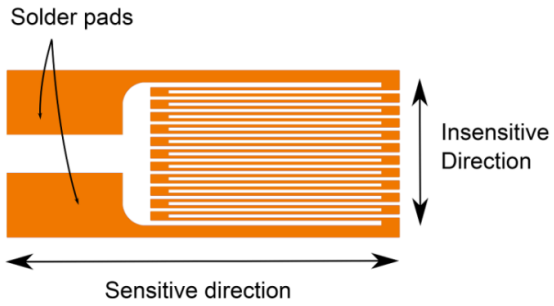

Figure 30. A principle sketch of a strain gauge. The sensitive direction produces a larger change in resistance when subjected to a deformation due to the length of the leads running in the direction of the strain.

Since only the deformation in the axial directions is of interest, the illustrated pattern is a perfect choice. The relation between the deviation in resistance and the causing strain is called the *gauge factor* and is defined as

$$GF = \frac{\Delta R}{R_0 \varepsilon}. \tag{36}$$

where ΔR is the difference in resistance, R_0 is the nominal resistance and ε is the strain. The gauge factor is tabulated for the specific strain gauge and is used to calculate the strain.

To measure the resistance, a so-called *Wheatstone bridge* is used, shown in figure 31. A voltage is applied over the bridge and the voltage between points B and D is measured. If the resistance of R_1,$R_2$and R_3 are known and R_x is that of the strain gauge, the strain can be calculated from the measured voltage V_g.

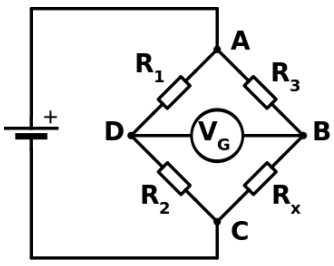

Figure 31.A Circuit diagram of a Wheatstone bridge.

If R_1,$R_2$and R_3 are the same as the nominal resistance of the strain gauge, the strain can be calculated as follows

$$\frac{V_G}{V_{ex}} = -\frac{GF\varepsilon}{4}\left(\frac{1}{1+GF\frac{\varepsilon}{2}}\right). \tag{37}$$

This signal is in the order of a 100 µV and one needs to amplify it to read it properly. A simple amplifier with a gain of 50 dB is used. This device uses accurate instrumentation amplifiers and includes a linear voltage regulator for the excitation voltage. The resistances used in the Wheatstone bridge are not perfect, since they come with a certain tolerance. In order to balance the bridge, so that the amplifier does not hit its rails, a potentiometer is used in series with one of the resistances. This also allows a resetting of the strain signal to neglect the strain coming from the preload.

3.7 Filtering

The signal from the strain gauge amplifier contains high frequency noise. This is due to the fact that the signal itself is small and heavily amplified. An initial hardware low pass filter, shown in figure 32, is implemented and connected between the amplifier and the DAQ-card. The highest frequency that is to be read is 10 kHz and the sampling rate is 120 kHz. When sampling a continuous signal at discrete points, a phenomenon known as *aliasing* might occur. High frequencies are mistaken for low frequencies due to the finite sampling. To reduce this, a rule of thumb is to attenuate the signal by a factor of 10 at the *Nyquist frequency*. The *Nyquist frequency* is half the sampling frequency, i.e. 60 kHz. A cutoff frequency of 20 kHz is chosen for the lowpass filter.

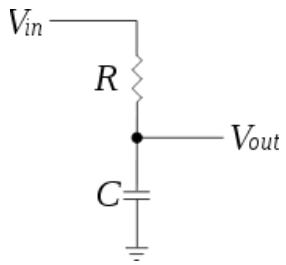

Figure 32. A first order lowpass filter.

By taking the Laplace transform of the output diveded by the input, one obtains the transfer function

$$\frac{\mathcal{L}\{y(t)\}}{\mathcal{L}\{x(t)\}} = \frac{1}{1+sRC}. \tag{38}$$

The cutoff frequency is defined as the frequency where this transfer function has the magnitude $1/\sqrt{2}$. This gives the cut-off frequency

$$f_c = \frac{1}{RC2\pi}. \tag{39}$$

By selecting a suitable capacitor, for example: $0{,}01\mu F$, the resistance that gives the desired cut-off frequency is $R = 795{,}77$. By picking a more realistic resistor, $R = 820$, the resulting cut-off frequency is $fc = 19409$ Hz.

Since the phase between the stress and strain is measured, this phase difference must remain unaffected by the filtering. By filtering the signal from the piezo sensor using the same filter both will experience the same phase lag and the phase difference will be unaltered.

3.8 Disturbances in strain signal.

Despite efforts made to suppress the disturbances of the system, the strain gauge signal is heavily contaminated, as shown in figure 33 (a). This signal is extremely sensitive. Since the signal itself is no more than 100 µV in amplitude and amplified by a factor 1000, noise is easily amplified, as well. In an attempt to counter this problem, the frequency of the filter is decreased. This does not remove the spikes, as seen in figure 33 (b), but greatly improves the result. One could increase the order of the filter to suppress the spikes further but this in turn affects the phase. Investigation reveals that the source of the disturbances is the SMPS and when the switching stops and the system operate on stored energy in capacitors, this issue completely disappears.

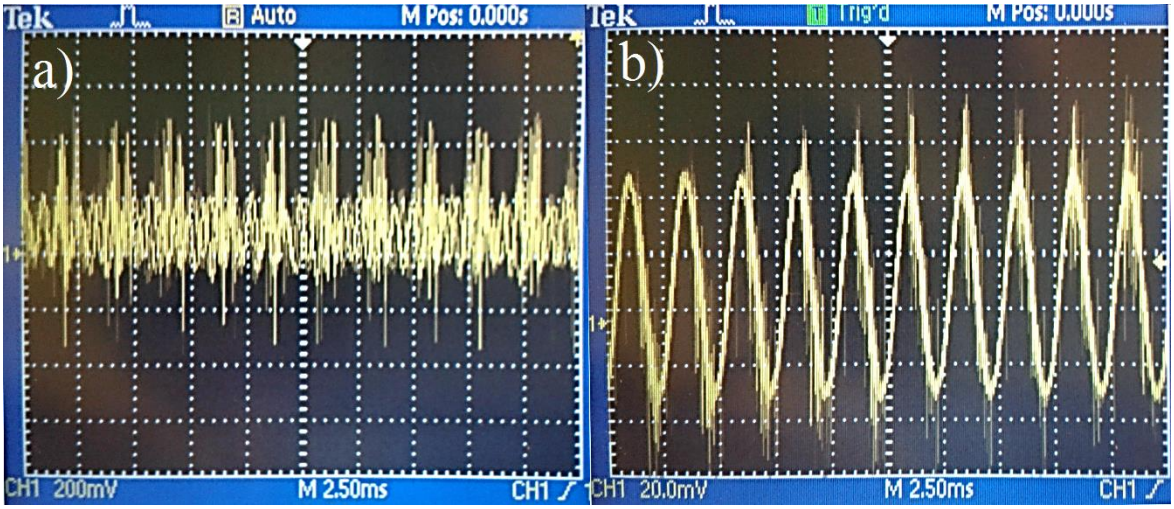

Figure 33. Signal from the strain gauge amplifier when the system is driven by the SMPS. a)Unfiltered signal. b)Signal filtered with 2kHz low pass filter.

It is decided to remove the SMPS completely and use other means to generate the high voltage. One approach is to use an external PSU to drive the power operational amplifier. This was implemented, but was not successful since the new PSU had the same noise issue and the unshielded cabling in-between gave rise to EMI. This simplified driver can be seen in figure 34.

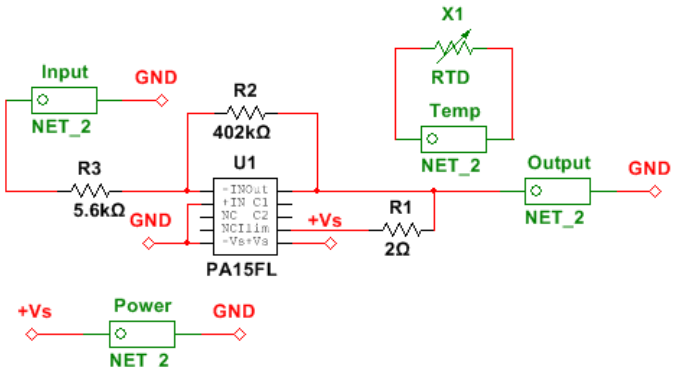

Figure 34 The simplified driver.

Instead, a piezo positioning device is used throughout the measurements that is virtually noise free, but lacks the desired power bandwidth, resulting in the measurements being done at low amplitude. This OWIS device has a capability of generating up to 500 V, but quickly loses amplitude with increasing frequency.

3.9 Piezo sensor

The piezo sensor is basically a disc made of piezoelectrical material, poled in the axial direction. For this application, the cables for reading the signal of the sensor must be connected in such a way that the surfaces are free. To solve this problem, a PCB is made with a footprint matching the size of the piezo disc, which is shown in figure 35. Additional solder pads are added to this PCB for the other sensors for strain relief on the cables. The sensor is covered with a thin copper foil, as depicted in figure 17. The piezo stack is later glued onto this sensor.

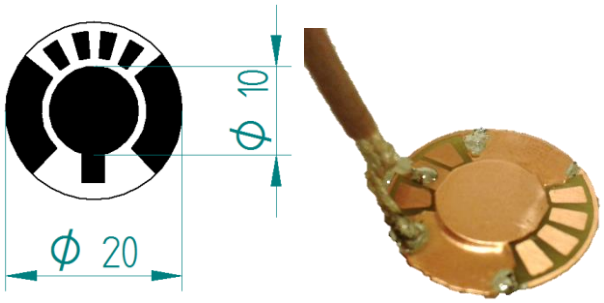

Figure 35. A PCB for connecting the piezo sensor. The PCB is etched using the footprint to the left.

4 SOFTWARE AND PROCESSING

This chapter describes the procedure of the measurements, the used equipment, the software and the created measurement interface. The post-processing of the data is also described.

4.1 Measurement equipment

A data-acquisition-card is used to measure the stress and strain signals, but also to generate a control signal to perform the frequency sweep. The highest frequency that is to be measured is 10 kHz according to the requirements. To properly read this signal, a rule of thumb is to sample 10 times faster, i.e., at least 100 kS/s. A suitable PCI-card that fulfills these requirements is purchased from National Instrument and is PCI6221, shown in figure 36.

Figure 36.DAQ-Card: PCI6221 and the custom-made Dsub connector.

This card has a sample rate of 240 kS/s, 16 analog inputs and 2 analog outputs. The sample rate is divided between the channels when measuring multiple signals, resulting in a channel sample rate of 120 kS/s for this application. Although this card does not support synchronous measurements, the effect this might have is negligible if the sample rate is high enough. This does create a time delay between the two measured signals and is discussed later.

This card is delivered with a 37-pin Dsub connector and a custom cable is made for the 3 signals, shown in figure 36. Since all signals are referenced to ground, single ended connections are used (GRSE). Coaxial cables are used to reduce the effect of EMI and BNC connectors are used.

4.2 Labview

A graphical user interface to control the measurements is constructed using Labview. Labview is a system design platform using visual programing and is a common engineering tool for these applications. For this project, components from the sound and vibration toolbox are used.

The general idea is to perform a frequency sweep across the measuring range and plot the amplitude and phase difference of the stress and strain signals.

The measurement range is divided into discrete measuring frequencies, either linearly or logarithmically. The user is prompted to input the upper and lower frequency limit, the number of sampling points, the measuring time and if the distribution should be linear or logarithmic.

A certain settling time is implemented at each frequency before the actual measurement is done. This is done so that transients that might occur when switching from one frequency to another do not affect the result.

The output amplitude and offset are set by the user and the corresponding driver voltages is displayed. Once these settings have been properly set, the user can initiate the measurement by clicking “start”. The current frequency, remaining time and the measured signals are displayed in real time. The interface is shown in figure 37.

The user is also able to make a reference measurement, so that following measurements can be compared to this reference. This reference is saved and exported to an external text file.

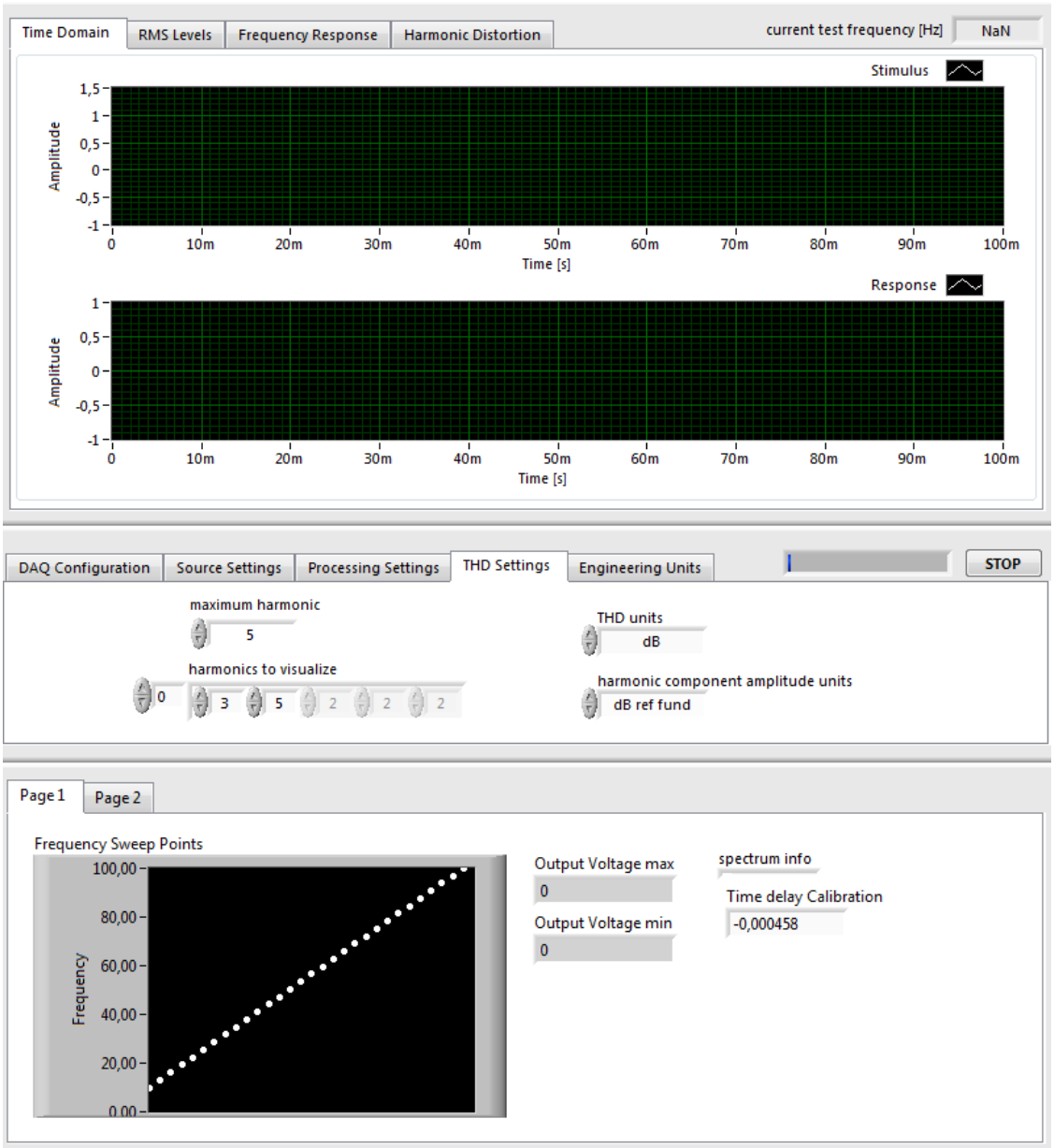

Figure 37. GUI of the Labview measurement program.

4.3 Temperature monitoring

The temperature sensors and the regulated voltage of the piezo driver are monitored by a Agilent 34970a Device, shown in figure 38. Using the provided software: “Agilent Benchlink Datalogger”, these values are measured once every second and plotted on a PC. Alarms are set if the temperatures reaches certain threshold values. The ambient temperature is monitored for refenrence.

Figure 38. The Digital Multimeter Device 34970a from Agilent.

4.4 Equipment set up

All the equipment is set up to run in parallel and is depicted figure 39. For explanations of the abbreviation, see the introduction.

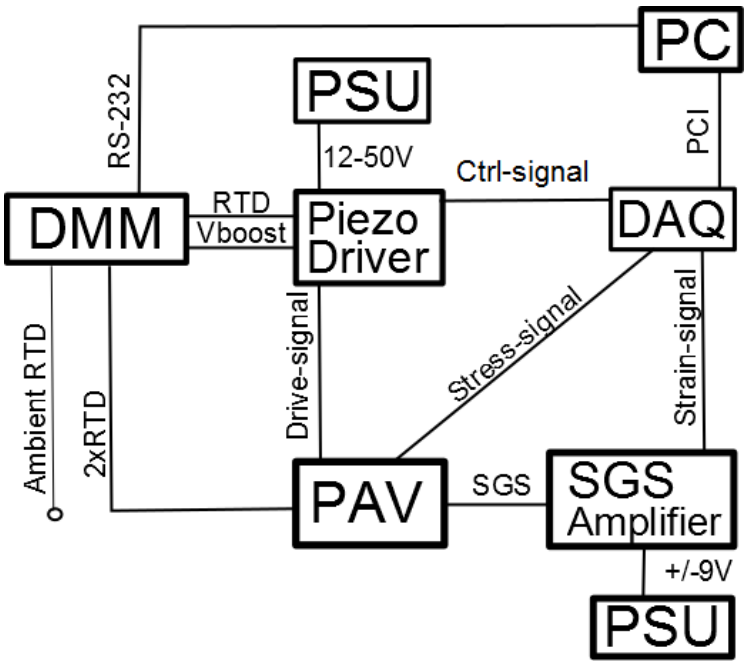

Figure 39. The equipment set up.

4.5 Verification

To ensure that the measurement equipment is providing accurate data, a measurement is performed on a first order low pass filter with known properties. This filter is made from a 82,5 Ω resistor and a 1 µf capacitor, resulting in a cutoff frequency of approximately 2 kHz. It can be seen in figure 40, that the amplitude is indeed -3 dB at this frequency. In fact, the entire amplitude curve is correct. For the phase however, it is expected to approach -90 degrees but instead it bends of at approximately 5 kHz. Further investigation reveals that this is due to a time delay in the DAQ-card. By deriving the frequency response when the input and output are connected together, this phase error can be measured. A time delay compensation is implemented removing this issue. The filter frequency response is redone, confirming a correct phase measurement.

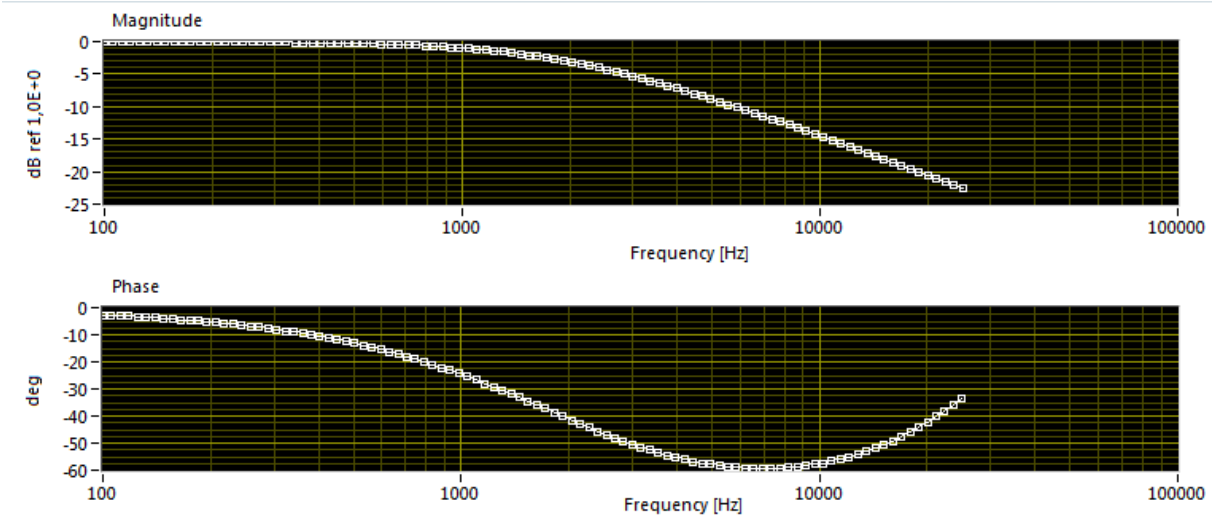

Figure 40.Frequency response of a 2 kHz first order low pass filter showing a phase error.

The piezo driver is tested, as well. With a peak-to-peak voltage span of 200 V and a load consisting of a 33 nf capacitor, it's frequency response is measured and shown in figure 41. This shows a very small drop in amplitude up to 10 kHz, but the phase decreases rapidly after 6 kHz. Neither the amplitude nor the phase actually affects the final measurement, since it is the frequency response of the stress and strain that is measured. The amplitude is needed, however, to obtain the proper displacement.

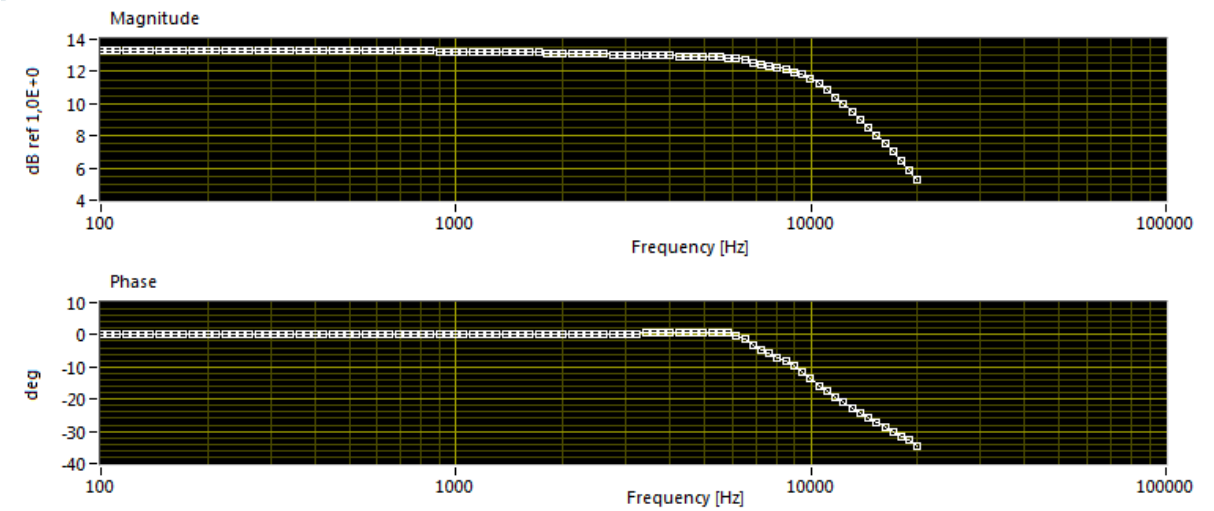

Figure 41. Frequency response of the piezo driver at 200V with a 33 nf load.

Finally, the response of the strain gauge amplifier is analyzed, see figure 42. It shows a fast response with an amplitude decrease of only 0,5 dB in 25 kHz. The amplification can be read out as approximately 50dB corresponding to a voltage amplification of about 330. There is a small phase decrease that can influence the result unless compensated for.

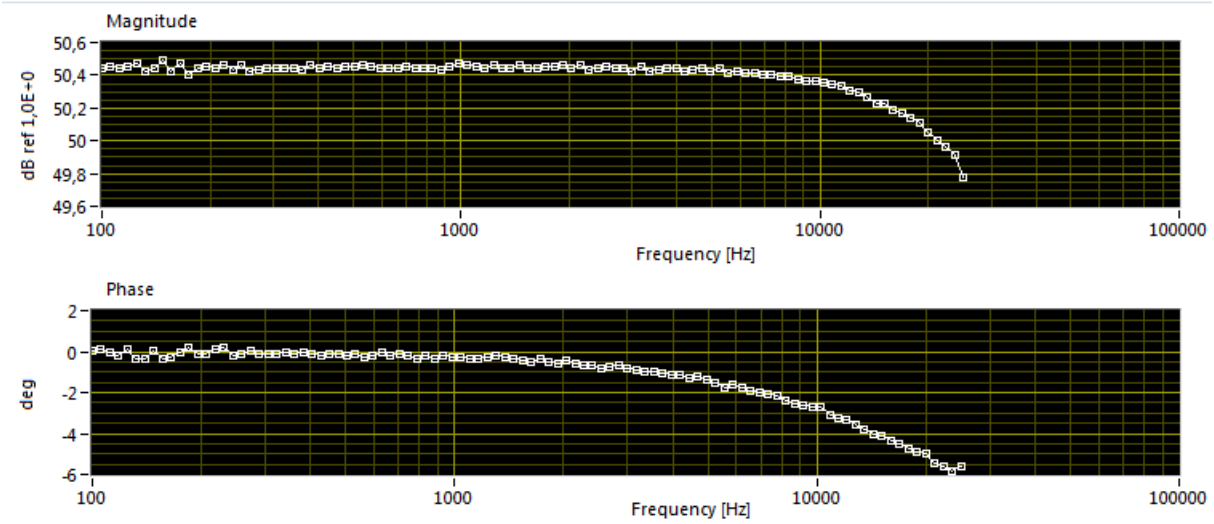

Figure 42. Frequency response of the SGS amplifier

4.6 Post processing of data

As stated in the introductory chapter, the rheological properties are often expressed as the storage and loss components of the complex shear modulus. The relation between the complex shear modulus and the complex spring constant is calculated using equation 16. The inverse of the complex spring constant is the complex compliance. If the dynamics of the system are neglected (k1 and k3 set to infinity in figure 11), this compliance is simply the ratio between the measured stress and strain

$$C = \frac{\sigma^*}{\gamma^*}. \tag{40}$$

The complex compliance can be expressed as

$$C^* = C' + iC'', \tag{41}$$

with the components

$$C' = \frac{\sigma_0}{\gamma_0}\cos(\delta), \tag{42}$$

$$C'' = \frac{\sigma_0}{\gamma_0}\sin(\delta), \tag{43}$$

where δ, is the phase difference between stress and strain and σ_0/γ_0 is the ratio between the amplitudes. The system dynamics cannot be neglected. Between 60 and 90% of the measured signal actually depends on the system itself. If the shear modulus is to be calculated, the mechanical parts need to be accurately modeled, which is not a part of this thesis. The mechanical equivalent set up in figure 11 is a good start, however.

In this chapter the results of the measurements are described, analyzed and discussed. The results are compared to what is expected by the theory described in the introduction, as well as the simulation results.

5.1 System dynamics

In order to verify that no resonance occurs in the measurement range, the dynamics of the system itself is measured. The sensors are placed in such a way that a measurement can be performed with no sample. This frequency response is derived using the stress and strain signals from the piezo sensor and the strain gauge respectively and is shown in figure 43. This response can be compared with the modal analysis in chapter 2. The modal analysis predicted a resonance of 7 kHz, which is what can be seen in figure 43. The torsional resonance mode at 11 kHz could be what cases the magnitude to decrease in this region. In order to reach 25 kHz, a lower amplitude is used.

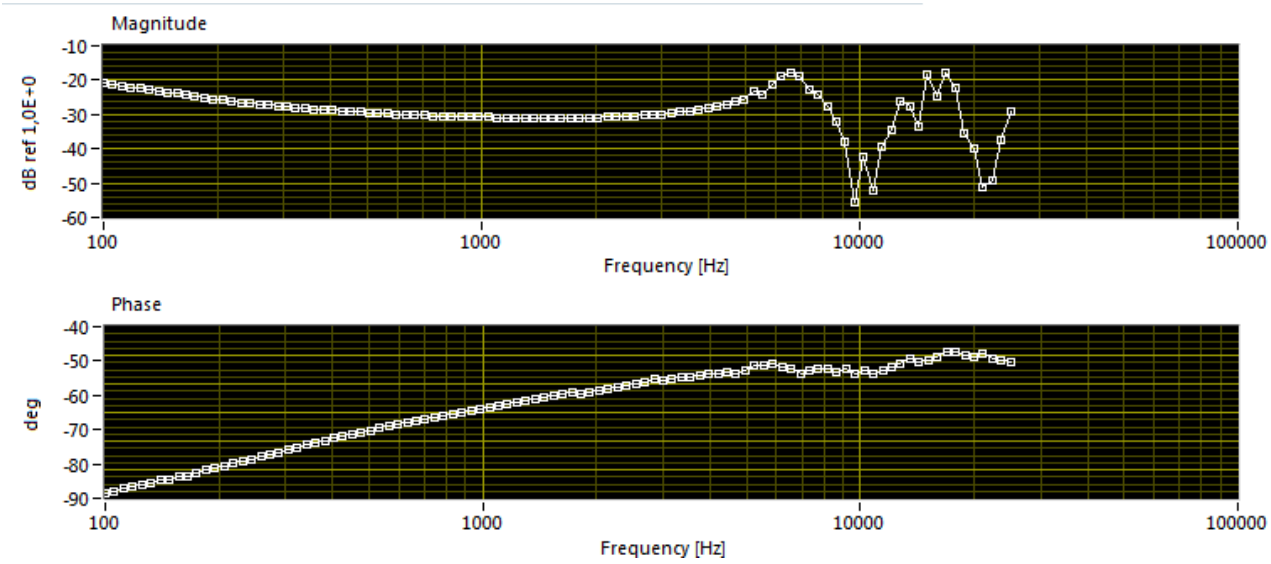

Figure 43. Frequency response of the unloaded system. This measurement is used as a reference.

5.2 Measurements

Since the dynamics of the system itself is of no interest when performing measurements on fluids, the deviation from a reference measurement with no sample is calculated, i.e. figure 43, for all measurements. In this way, the influence from the sample is isolated and easier to illustrate and compare. Actually, the majority of the signal originates from the system dynamics, making this type of action necessary in order to assess the result. It should be noted, however, that this is performed only to illustrate the results. If the actual shear modulus were to be calculated the system dynamics cannot simply be subtracted. These measurements are made more as a proof of concept than to produce accurate predictions.

5.3 Repeatability

To assess the reliability and to see to what extent the system is influenced by noise, the repeatability of the measurements is studied. Multiple measurements are conducted on the unloaded system and the deviation from the average is studied. Figure 44 shows this average deviation for the phase and amplitude measurements. It can be concluded that the result is consistent in the interval 300-5000 Hz fluctuating less than 1%. Below 300 Hz, there appears to be some sort of disturbance producing an average deviation of up to 5%. This has a large impact on the result since only 10-40% of the measured results depend on the fluid.

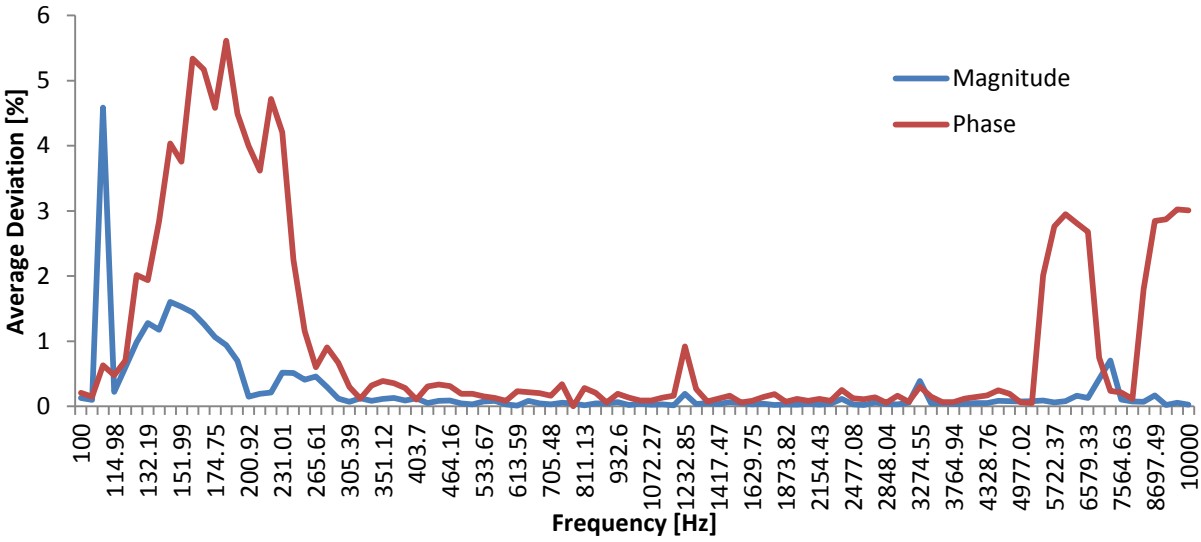

Figure 44. Average percentage deviation in the phase and amplitude measurement from a reference for 5 consecutive reference measurements.

5.4 Testing fluids

To test the rheometer, silicone fluids from the chemical company Wacker is used. Six different silicone fluids are tested, with viscosities ranging from 10 mPas to 100 Pas and are listed in table 3. These are highly stable and inert substances with properties tabulated with great accuracy. At low viscosities these fluids behave as Newtonian, i.e. following equation 2, but past 1 Pas they start showing shear thinning properties. Another testing fluid, called AR1000, with a different chemical formula is added for comparison.

Table 3. Testing fluids

Fluid	Dynamic viscosity [mPas]	Density [g/cm3]
Ak10	9,3	0,93
AK200	193	0,966
AR1000	~1000	0,97
AK2000	1940	0,97
AK10000	9700	0,97
AK30000	29100	0,97
AK100000	97000	0,97

5.5 Pre shear

Investigation shows that when making multiple consecutive measurements on a fluid, the response consequently decreases. This could be due to the vibrations of the measurements are actively redistributing the sample. Multiple measurements on the fluid AK2000 are shown in figure 45. It can be seen that the biggest response comes from the first measurement and decrease with the following measurements. This phenomenon has a tendency to decrease with higher viscosity, which supports the proposed explanation. It can also be seen that for a certain number of measurements, the response reaches a steady value. It is believed that when this happens, the fluid has reached an optimum distribution on the lower plate. To increase the accuracy of the measurements and to remove the spread in the result, each measurement is initiated by vibrating the sample thoroughly at 10 kHz. This reduces the spread in the result but does not remove it completely. Instead 20 "dummy" measurements are made before actually looking at the results. The result of this action is shown in figure 46. It can be seen that the curves completely overlap, except for some minor static for the six measurements. This technique is applied for all measurements and the average of six measurements is used.

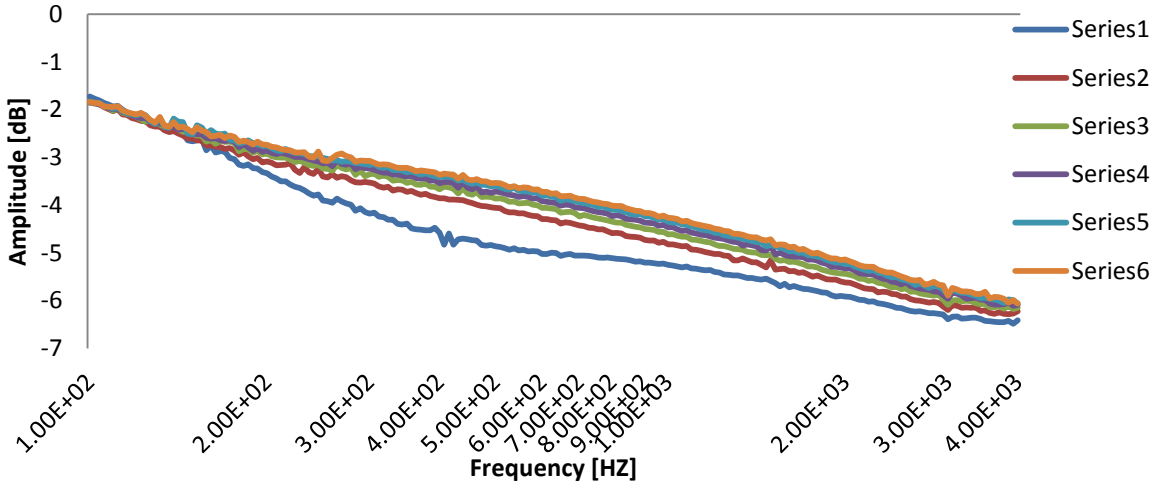

Figure 45. Spread in the result when making multiple consecutive measurements.

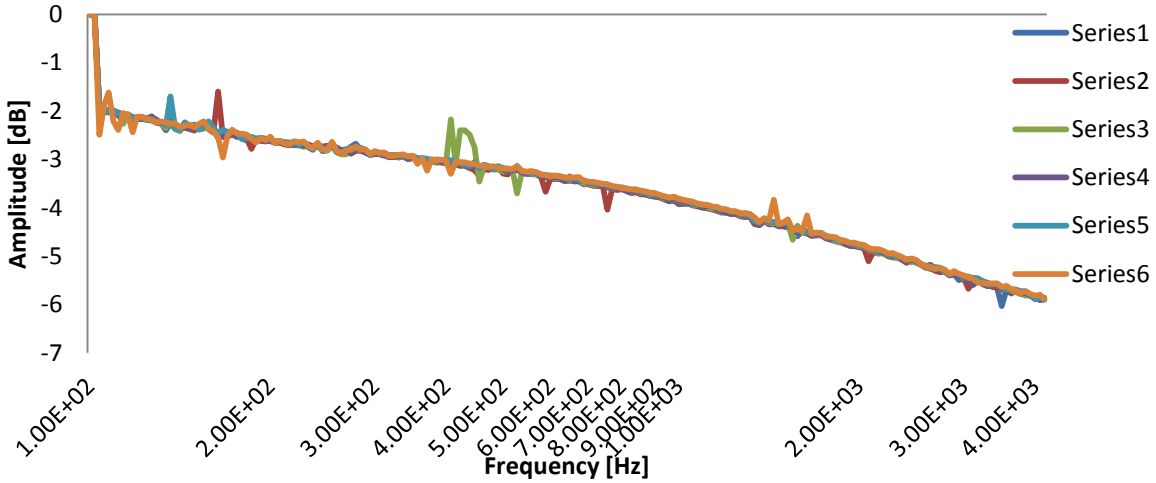

Figure 46. Spread in the result after 20 "dummy" measurements.

5.6 Silicon oils

The results from the measurements made on the seven silicon oils are plotted in the same graph, shown in figure 47 and 48, for the same test conditions. A 150 µm spacer is used and 180 V driving voltage. The frequency sweep is done from 100 to 4 kHz.

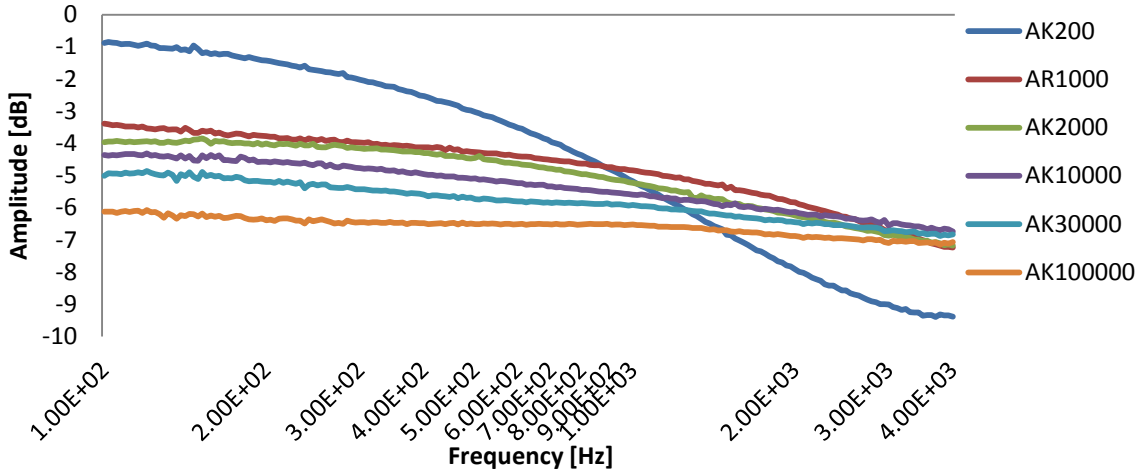

Figure 47. The amplitude difference from a reference for the seven silicon oils.

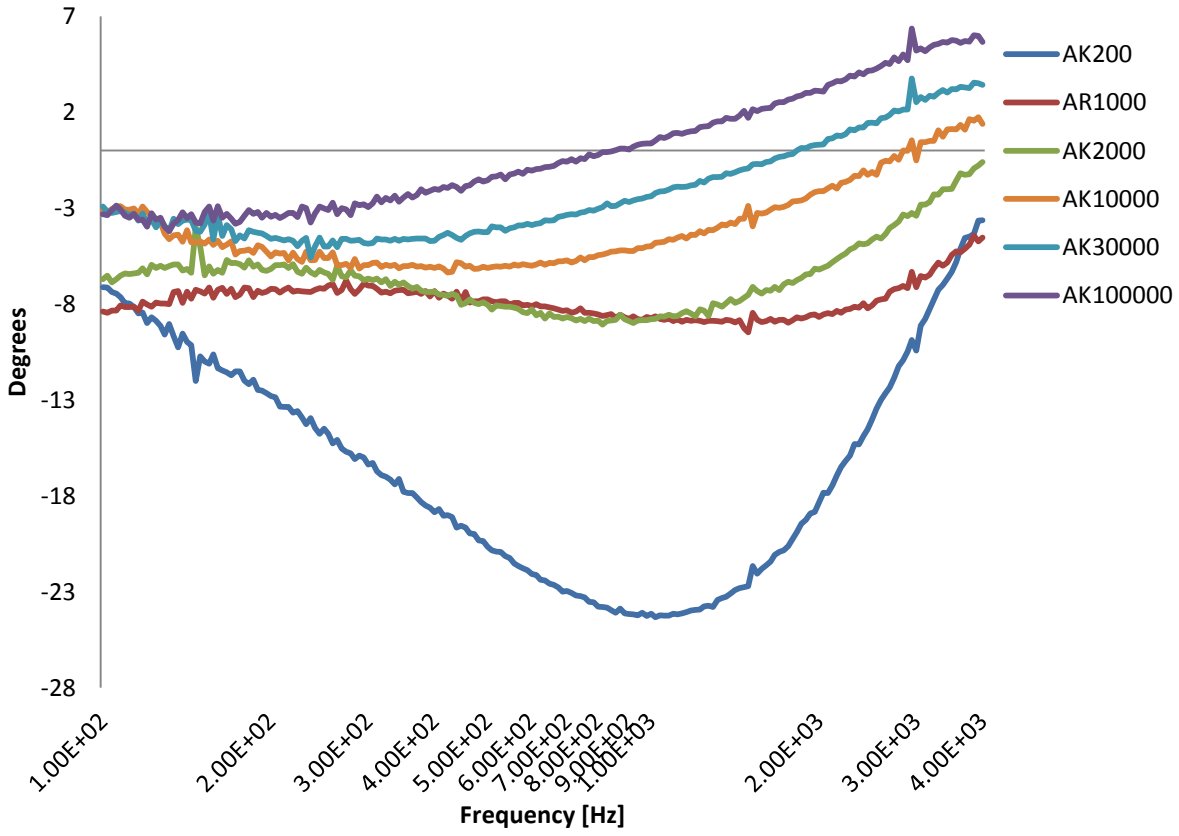

Figure 48. The difference in phase for the seven silicon oils.

In figure 48, it may be noticed that one of the fluids seems to behave differently. AR1000 is not showing the same general appearance as the rest of the fluids and this is most likely due to its different chemical structure. There seems to be a gap between AK200 and the rest of the fluids.

5.7 Complementary silicon oils

To investigate the properties of the fluids between AK200 and AK2000, new testing fluids are produced by mixing these in different proportions.

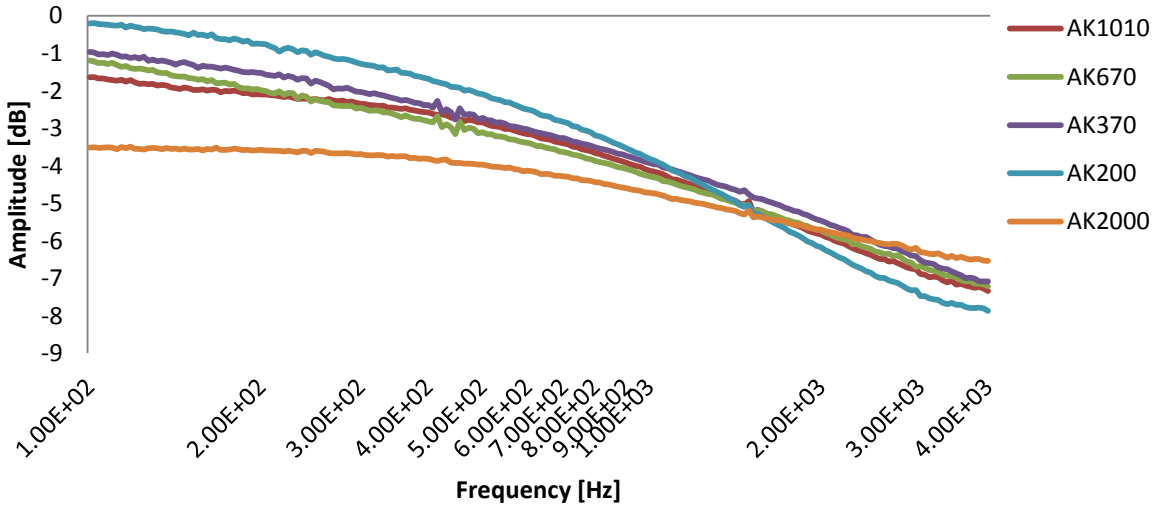

Figure 49. Amplitude difference for AK200, AK2000 and the three new silicon oils in between.

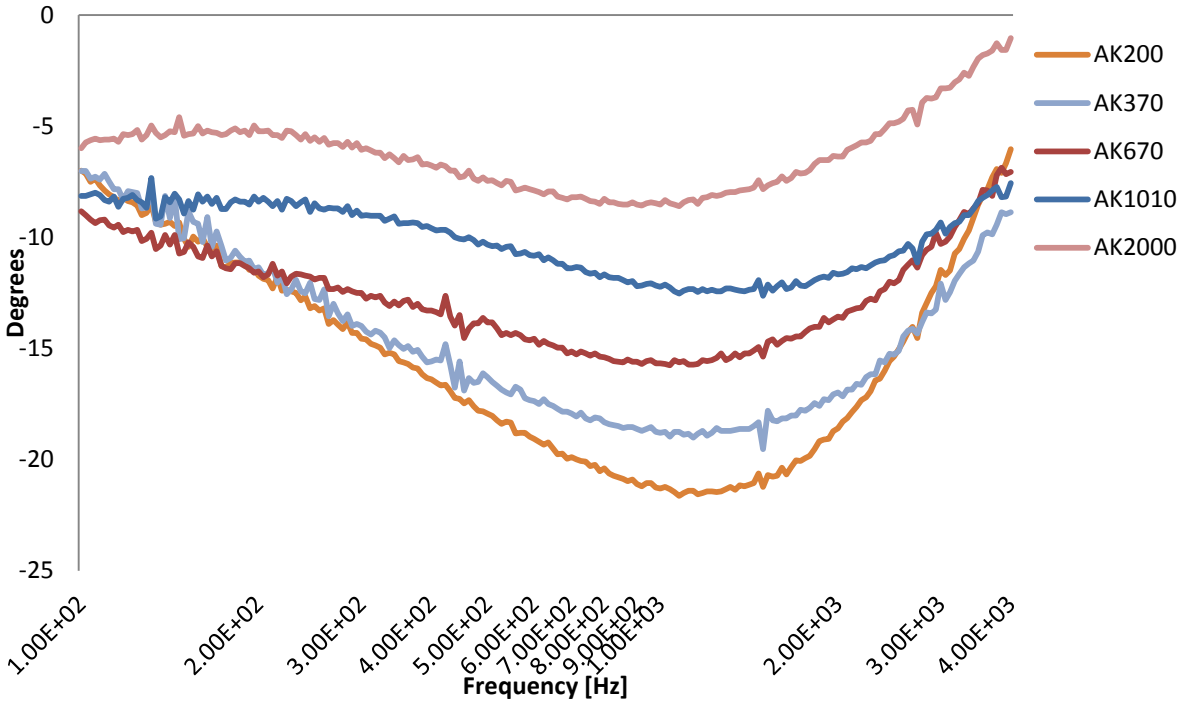

Figure 50. Phase difference for AK200,AK2000 and the three new silicon oils in between.

It can be seen that the fluids continue the pattern laid out in figure 47 and 48. Therefore, it can be concluded that the AK-type silicon oils have a very characteristic response, which differentiate it from the AR-type silicon oils. The plot in figure 49 and 50 fits perfectly in the gap revealed in figure 47 and 48. Although these lower viscosities have a greater difference in their response, they also show a greater difference between the measurements, making it difficult to make conclusions about in what region the resolution is best.

5.8 Adhesive test

As stated in the introduction, there is an interest in jetting different types of fluids, such as adhesives. To test the rheometer's capability to characterize these fluids, two different epoxy adhesives are tested, manufactured by Loctite and Hereaus, respectively. Two complete tests are made on both fluids, i.e. the fluid is removed and reloaded in between measurements. Their amplitude and phase difference from a reference measurement is plotted in figure 51 and 52.

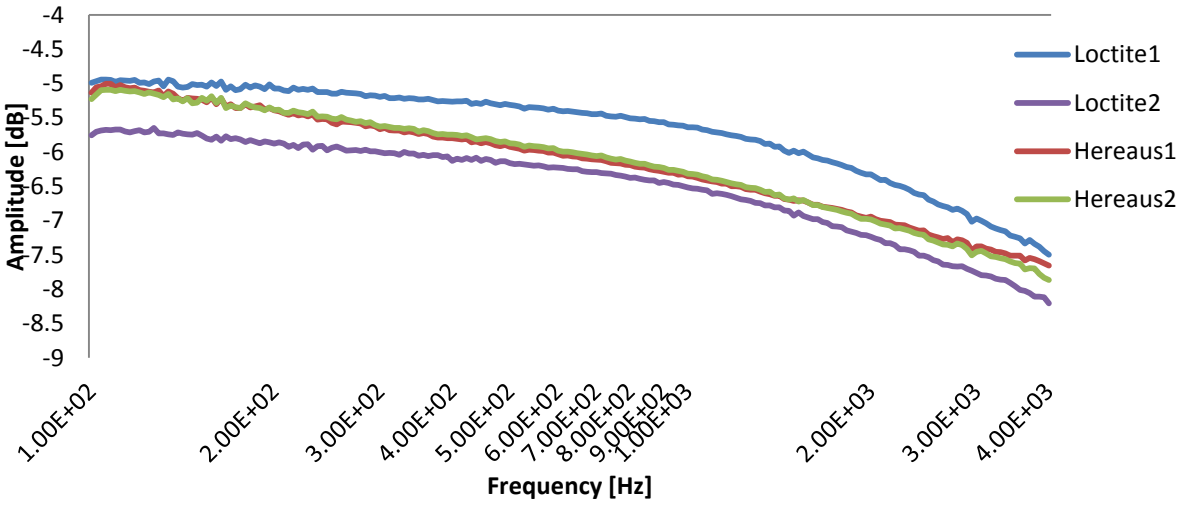

Figure 51. Amplitude difference for two epoxy adhesives.

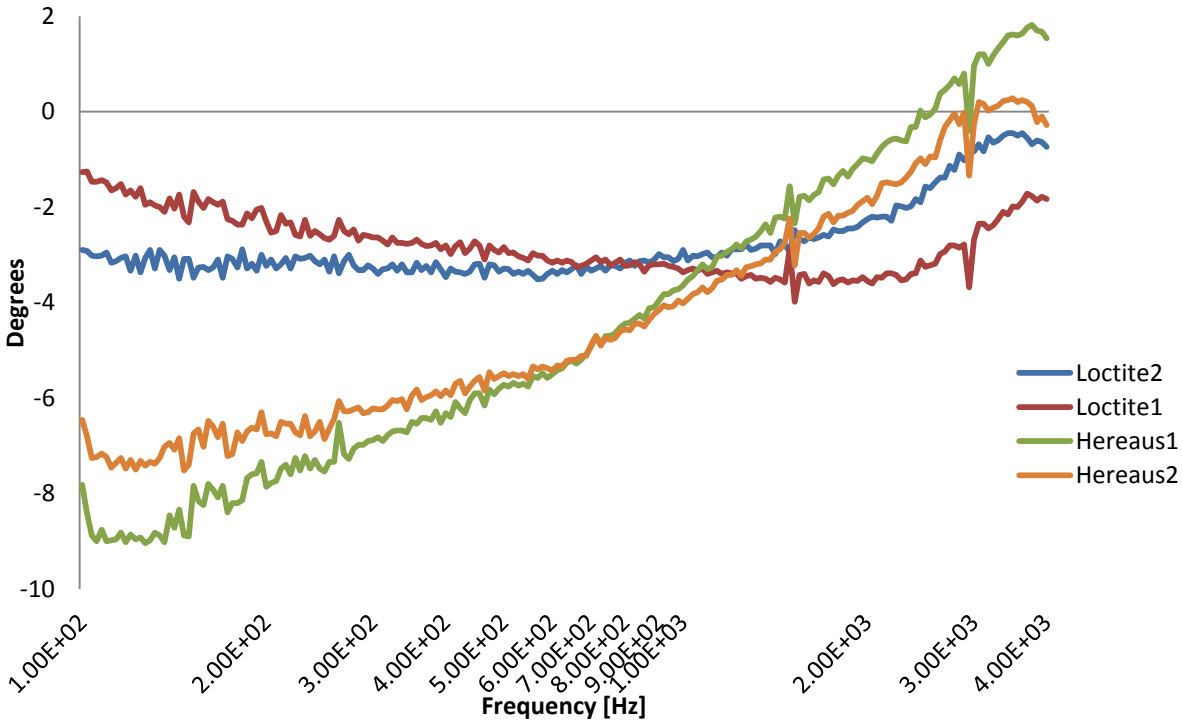

Figure 52.Phase difference for two epoxy adhesives.

It can easily be seen that these fluids behave differently. Except for an offset in one of the curves, in figure 51, both measurements show similar results. These measurements are compared to the result obtained using a rotational rheometer, which indicate the same result. With increasing shear rate the Hereaus adhesive changes its properties in a greater extent.

5.9 Solder paste

As expected, the solder pastes are very similar and their differences are expected to appear at high shear rates. Since there is no simple conventional rheometer capable of measuring at high shear rates, there is no definite answer to how these fluids will behave. Five different solder pastes are tested twice and their deviation from a reference is plotted in figure 53 and 54. The tests are made in a random order to increase reliability.

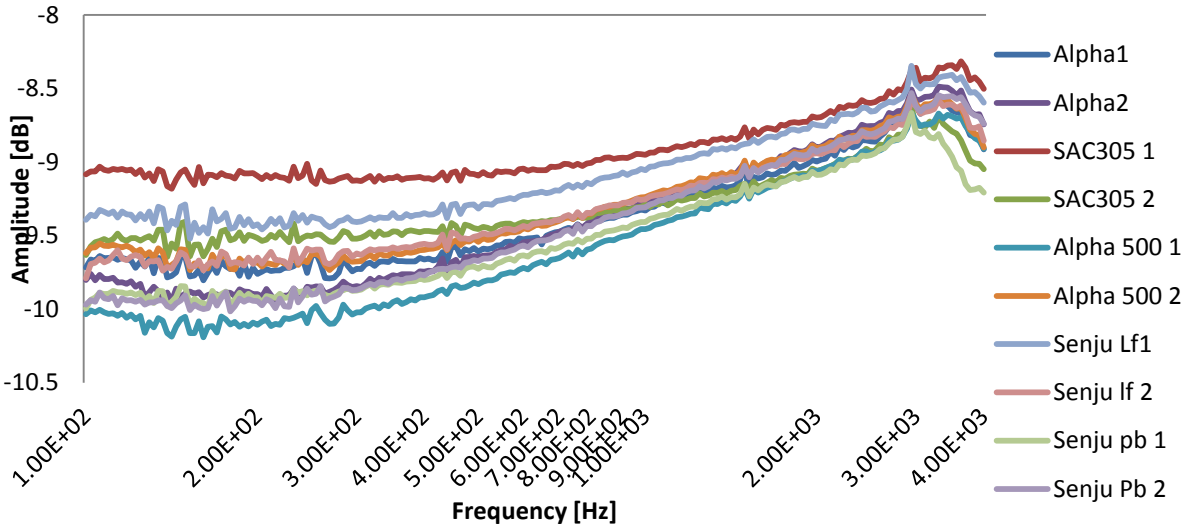

Figure 53. Amplitude difference for five solder pastes.

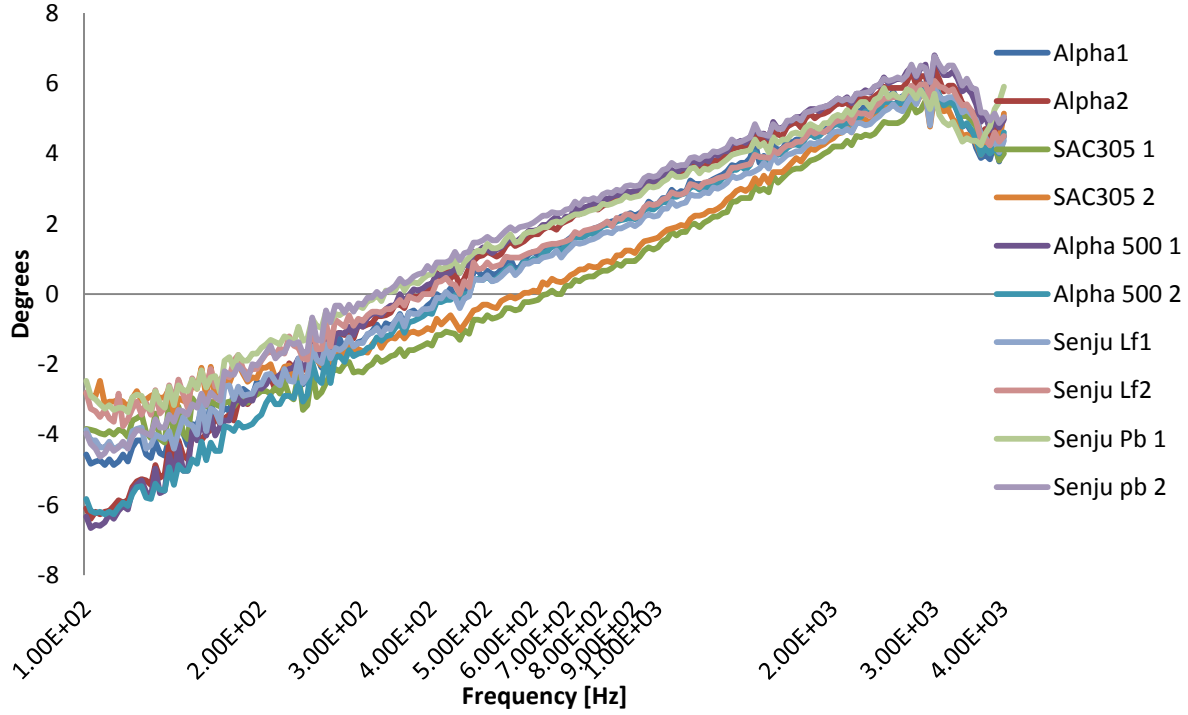

Figure 54. Phase difference for five solder pastes.

No conclusions should be drawn about deviations that are less than the spread in the result. Since the amplitude curve easily can be offset and their typical appearance seems to be the same, no conclusion based on this plot should be drawn. In the phase plot however, the SAC305 paste clearly stands out with both its measurements, indicating a possible difference in its rheology.

5.10 Spacer sizes

The effects of having different spacer sizes are investigated and as a reference the fluid AK10000 is used. The same test conditions are used for all cases and the results for five different spacers are shown in figure 55 and 56.

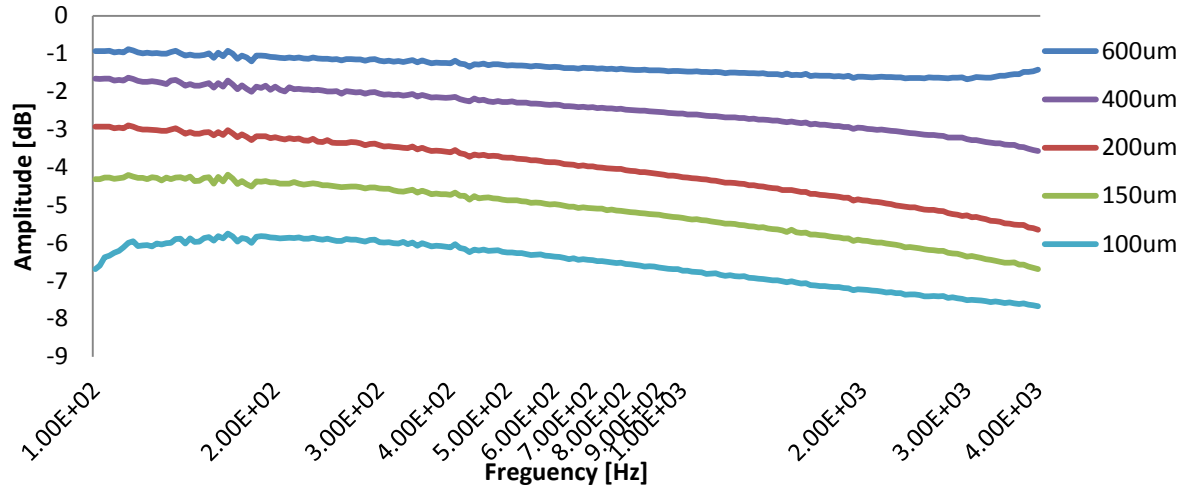

Figure 55. Amplitude difference for the measurements with five spacer sizes for the fluid AK10000.

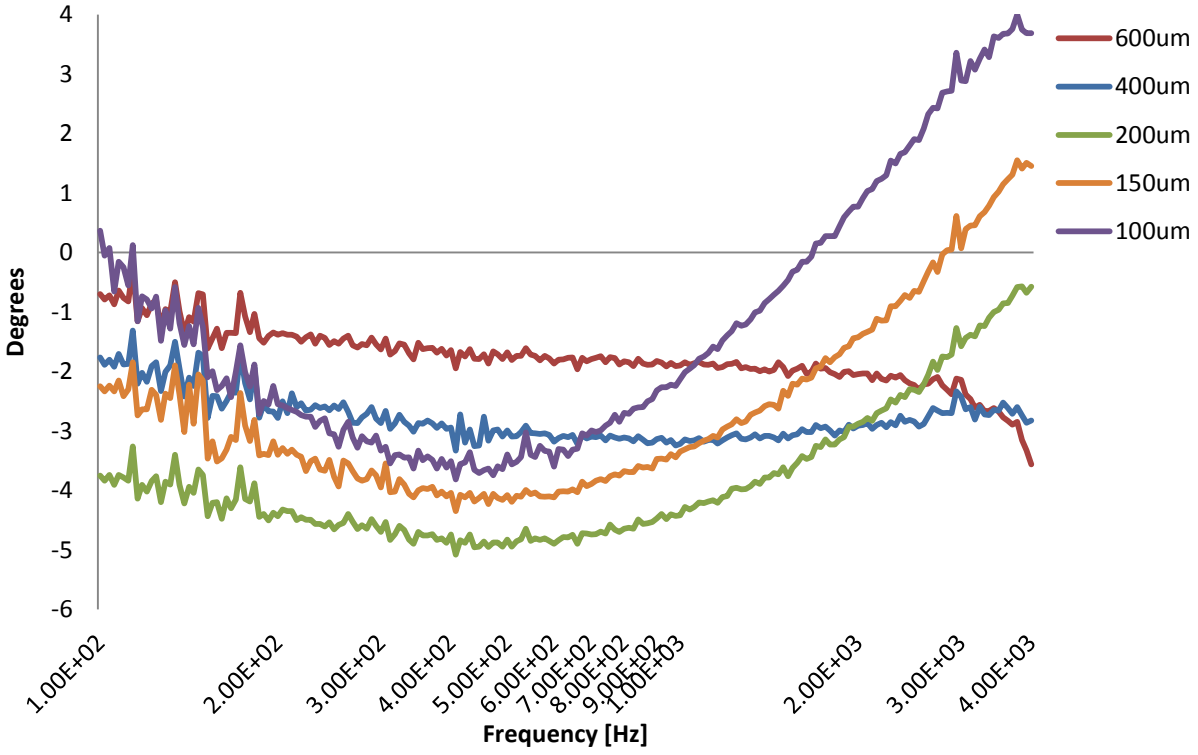

Figure 56. Phase difference for the measurements with five spacer sizes for the fluid AK10000.

As expected, the response gradually increases when the distance between the plates is lowered. Having a smaller spacer actually increases shear rate, since the deformation is distributed on a smaller volume. The phase curve shows the effects of this increase in shear rate, as this is a shear thinning material. As the frequency goes up, the shear rate increases and the difference due to the different spacer sizes becomes clearer.

5.11 Amplitude test

The effects of changing the driving voltage and consequently the amplitude have also been investigated. If the voltage is increased, the amplitude of the deformation increases, as well. This is not expected to change the amplitude difference between the stress and strain, since this relation depends on the dynamics of the system and the properties of the fluid. With higher amplitude the shear rate is increased, which governs how the fluid behaves. The result, shown in figure 57 and 58, shows the response for eight different driving voltages. At low frequencies, when the shear rate is low, the result is expected to overlap. This is not the case, however. Since these plots depict a difference from a reference, the scaling might be different, which leads to the spread in the result. The result seems to converge with increasing voltage.

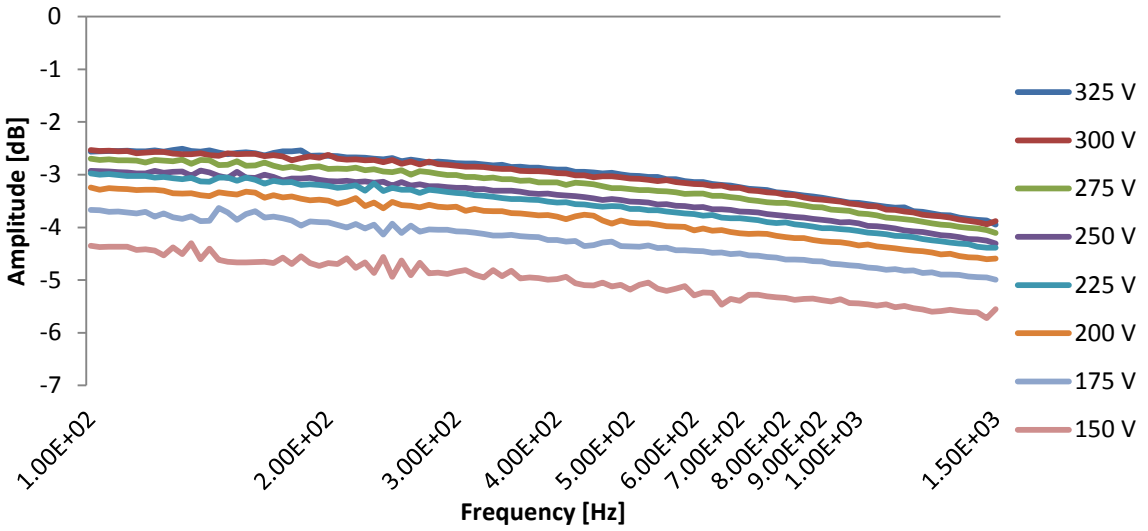

Figure 57. Amplitude difference for eight different driving voltages for AK10000

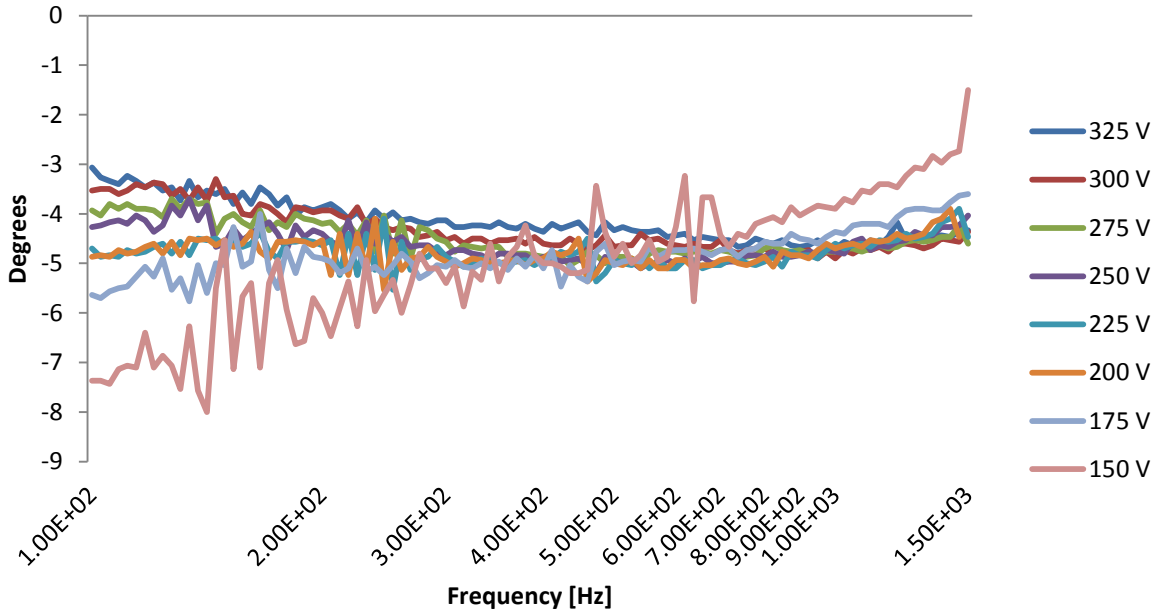

Figure 58. Phase difference for eight different driving voltages for AK10000

With higher amplitudes the signal to noise ratio is improved, which is reflected by the decreasing noise in both the amplitude and phase response.

6 DISCUSSION AND CONCLUSIONS

A discussion of the results and the drawn conclusions are presented in this chapter. Based on the results presented in chapter 5, the rheometer is evaluated and verified with respect to the requirements and validated with respect to its goal.

6.1 Verification

Making oscillatory measurements with a frequency of 10 kHz turned out to be extremely difficult. A compromise was made when manufacturing a design with a resonance frequency of 7 kHz. Measuring the phase difference at this high frequency also posed a challenge. With the equipment used, it is shown that values above 4 kHz should be considered less accurate. Repeated issues with noise in the measured signals have limited this frequency range. And most of the electronics should be revised to improve this. Making a piezo driver capable of reaching this high frequency at a high voltage was done, but proved unusable due to noise.

The temperature was never an issue since the current piezo driver had a low power bandwidth. The temperature of the piezo stack only increased a few degrees which left the temperature of the plates unaffected. Cooling was therefore never required.

The rheometer was tested for viscosities ranging from 10 mPas to 100 Pas, which was two orders of magnitude short of what was stated in the requirement, but these values could easily be tested as well. Lower viscosities actually showed a larger change in the frequency response.

6.2 Validation

The rheometer has shown great potential in characterizing fluids at high shear rates. The results show a great sensitivity for viscosity of many orders of magnitude. Although the characterizing of solder pastes proved to be a challenge due to their similarity, is it shown that some differences can be detected. Further work should be done for improving the accuracy.

Since only the phase and amplitude values of the piezo stack are available from the measurements, it is impossible to make any accurate predictions using this system as it is. It can be concluded that the repeatability is good and therefore the difference in result must be due to the sample. The result is affected by the dynamics of the mechanical parts in a non-linear way making the difference between the silicon oils in figure 47 and 48 not necessarily correspond to their viscosity.

A reoccurring issue with the measurements is that the curves easily get offset relative to each other. This is believed to be caused by the strain signal that has a tendency to drift. This is mainly present in the amplitude curves. The figures show that it is the phase curve that is most prone to change with increasing shear rate and consequently relates the most of the fluids change in behavior.

Although fluids with similar viscosity show similar response at low shear rates, their amplitude and phase curves can be completely different. This can be seen when comparing AR1000 with AK1010 revealing a clear difference.

There are currently no rheometers of this kind on the market and this thesis adds to the research made on similar devices. As stated in the introduction, rotational rheometers are limited with respect to their shear rate. To utilize capillary rheometers would be not be an option when using expensive materials. Having a working rheometer of the type developed in this thesis would be invaluable for these applications since it uses only a small volume of the material. The measurement procedure is also very simple making it possible to conduct a measurement in just minutes.

The simplicity of the device could also make this type of device very cost effective. The electronics could easily be implemented in compact cost effective design. Extrusion rheometers are both large and expensive in comparison.

The loading procedure is identified as one of the bigger error sources for this device.

7 RECOMMENDATIONS AND FUTURE WORK

In this chapter, recommendations and possible future work is described. It covers what needs to be done to improve accuracy, measuring frequency and the assessment of the data.

7.1 Post processing

It was decided early on that due to time limitations the work on post processing the data in order to find the complex shear modulus would not be a part of this thesis. Although the procedure is described in the introductory chapter, the relation between the complex shear modulus and what is measured is complicated. A thorough calibration work would have to be done and one would possibly have to consort to intelligent system identification algorithms.

7.2 Electronics

A reoccurring problem in this thesis is noise which prevents accurate phase measurements. There are two ways of solving this issue: Either removing the source of the noise or by filtering the contaminated signal. The latter would need a very steep pass band filter that does not affect the phase. A lock-in amplifier would be ideal for this purpose: By detecting the frequency of the exciting signal and filtering the noisy signal with a narrow pass band filter centred at this frequency an extremely high signal to noise ratio can be achieved.

The amplification of the strain signal should also be revised. A shielded amplifier together with short cables would be ideal. Another "dummy" strain gauge should be attached in order to obtain a temperature compensation for the measured strain. The potentiometer used for balancing the bridge should be replaced with high tolerance resistors. A phase neutral amplifier is also favourable.

A noise-free piezo driver with a high power bandwidth is also something that could be worth acquiring for future use of this device.

A DAQ-card with a higher sampling frequency and simultaneous sampling would increase the accuracy and remove the issue with the time delay. The card currently used is a low end card not intended for this type of application.

7.3 Temperature controlled measurements

As stated in the introduction, the viscosity is highly temperature dependent and controlling the temperature has not been addressed in this project. Even though the temperature is kept constant for each measurement, the data is only valid for this specific temperature. The temperature could be controlled by implementing a circulating water bath to cool or heat the outer surfaces of the rheometer. For the purpose of characterizing solder paste to assess their jetting behavior, the ideal case would be to measure this at the temperature usually occurring during jetting.

7.4 Loading mechanism

As stated earlier the loading procedure is a critical step and investigation shows that the result is strongly affected by how the sample is loaded. For viscoelastic substances, such as solder paste, the material retains its structure, making it prone to encapsulate small pockets of air. To minimize this risk and to remove the human factor, a mechanical loading mechanism could be constructed. A fairly simple solution is depicted in figure 59 making use of the rheometer designed in this thesis.

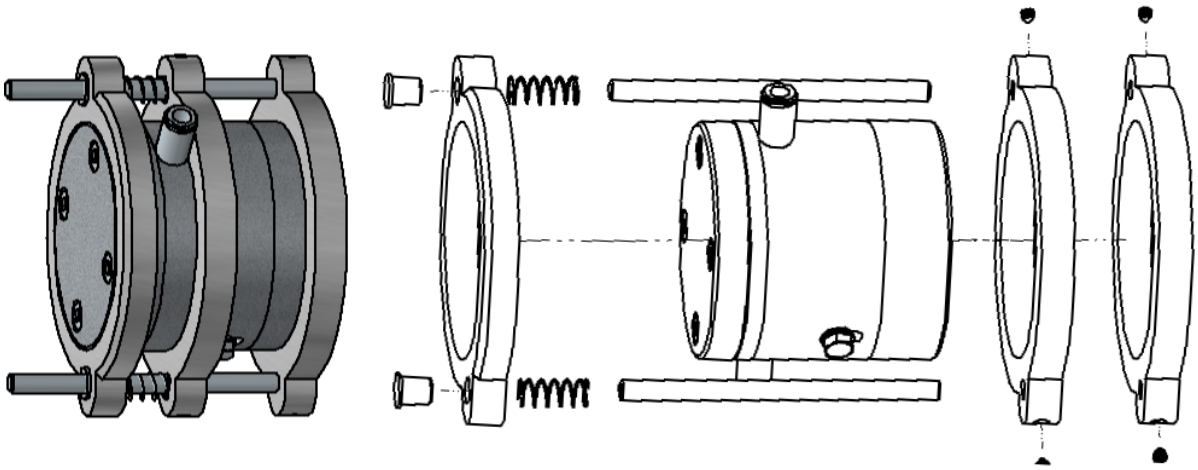

Figure 59. A guiding rail for the loading procedure

7.5 Relaxation time

Another rheological property that could be measured using this device is the relaxation time of the fluid, i.e. the time for the fluid to reach equilibrium in response to an external perturbation. If the fluid is repeatedly exited by an impulse from the actuator and the response is monitored, the relaxation time can be found by gradually reducing the time between the impulses until the response start showing influence of previous impulses.

7.6 Labview interface

At present, the measurements are time consuming in the sense that an operator is required for each step of the process. This whole process could easily be automated. The Labview program could be set to perform the entire set of actions, including pre-shear, measurement, averaging and post processing.

8 REFERENCES

Crassous, J., R. Régisser, M. Ballauff, and N. Willenbacher *"Characterization of the viscoelastic behavior of complex fluids using the piezoelastic axial vibrator,"* J. Rheol. 49, 2005, pp. 851–863.

D. C. Vadillo, T. R. Tuladhar, A. C. Mulji, and M. R. Mackley, *"The rheological characterization of linear viscoelasticity for ink jet fluids using piezo axial vibrator and torsion resonator rheometers",* J. Rheol. 54, 2010, pp. 781-795.

Kirschenmann Ludwig, *"Aufbau zweier piezoelektrischer Sonden (PRV/PAV) zur Messung der viskoelastischen Eigenschaften weicher Substanzen im Frequenzbereich 0.5 bis 2kHz bzw 0.5 bis 10kHz",* Ulm, 2003.

Jan Engmann, Colin Servais, Adam S. Burbidge, *"Squeeze flow theory and applications to rheometry: A review",* J. Non-Newtonian Fluid Mech. 132, 2005, pp 1–27.

T. A. Nguty, N. N. Ekere *"Modeling the effects of temperature on the rheology of solder pastes and flux system"*, Journal of materials science: Materials in electronics 11, 2000, pp 39-43.

H.A.Barnes., J.F.Hutton. and K.Walters*.,"An introduction to Rheology",*1989.

Thomas G. Mezger, *"The Rheology Handbook"* 3rd edition,2011.

Physik Instrumente, *"Piezoelectrics in positioning"*, http://www.physikinstrumente.com/en/pdf_extra/2009_PI_Piezo_University_Designing_with_Piezo_Actuators_Tutorial.pdf, accessed 2014-04-22.

Physik Instrumente, *"PICA Power Piezo Actuators"*, http://www.physikinstrumente.com/en/pdf/P010_xxP_Datasheet.pdf, accessed 2014-04-22.

Piezo Technologies*, "Usage Temperatures of Piezoceramic Materials",* http://www.piezotechnologies.com/Resources/White-Papers/Usage-Temperatures-of-Piezoceramic-Materials.aspx, accessed 2014-04-22.

Apex Microtechnologies,*"Driving Piezoelectric Actuators",* http://www.apexanalog.com/wp-content/uploads/2012/10/AN44U_3.pdf, accessed 2014-04-22.

Apex Microtechnologies,*" Driving Capacitive Loads",* http://www.apexanalog.com/wp-content/uploads/2012/10/AN25U_G.pdf, accessed 2014-04-22.

Apex Microtechnologies,*" Power operational amplifiers (MP400)",* http://www.apexanalog.com/wp-content/uploads/2012/10/MP400U_F.pdf, accessed 2014-04-22.

Apex Microtechnologies,*" Power operational amplifiers (PA78)"*, http://www.apexanalog.com/wp-content/uploads/2012/10/PA78U_E.pdf, accessed 2014-04-22.

Vishay Precision Group*"Strain Gage Selection:Criteria, Procedures, Recommendations",* http://www.vishaypg.com/docs/11055/tn505.pdf, accessed 2014-04-22.

Vishay Precision Group, *"Noise Control in Strain Gage Measurements"* http://www.vishaypg.com/docs/11051/tn501.pdf, accessed 2014-04-22.

National Instruments, *"Measuring Strain with Strain Gages",* http://www.ni.com/white-paper/3642/en/ , accessed 2014-04-22.

Maxim Integrated, **"***Filter* Basics**:** *Anti-Aliasing*", http://www.maximintegrated.com/app-notes/index.mvp/id/928, accessed 2014-04-22.

Omega *"What are RTD sensors?",* http://www.omega.com/Temperature/pdf/RTD_Gen_Specs_Ref.pdf, accessed 2014-04-22.

Micronic Mydata, "*MY500 Brochure*" http://www.mydata.com/www2/elements.nsf/(read)/8C86B8F03441C639C12577A7006B3EDB/$file/MY500%20Brochure%20P-001-0218.pdf, accessed 2014-04-22.

APPENDIX A: Requirements

User requirements

The rheometer shall measure the viscosity of viscoelastic fluids for frequencies between 100-10000Hz.
The rheometer shall measure viscosities in the range 1mPas-1kPas
Colloidal substances with a particle size of less than 25m shall be measured. The particles are considered as hard spheres.
The temperature of the measurements shall be done between 20-35 °C with a deviation during measurement of less than 0.5 °C.
The stiffness of the rheometer must be measured.
The rheometer may be used to find relaxation times of fluids.

System requirements

The sensor piezo element shall be placed such a way to that allows measurement on the system dynamics.
Temperature controlling must be implemented.
The gap size shall be at least 10 times the size of the particles.
A variation of gap sizes may be used to get more accurate results for different viscosities.
A user friendly loading mechanism may be implemented.
A glass lid for visual input on the sample may be considered.

Electronics

Piezo driving electronics must be implemented with the capability of reaching the desired frequency.
The user must be protected against high voltage.
The data must be filtered preferably using a lock-in-amplifier.
The data must be sent to a computer for processing and amplified if necessary

Software:

Data of the amplitude difference and the phase difference will be used derive the loss and storage modulus of a Maxwell model.
A calibration process in finding the correct gap size must be done.
The parameters of the unloaded system must be found making a measurement of the unloaded system.
A periodic excitation with a constant frequency followed by different resting times may be considered when finding the relaxation time of the fluid.
The rheometer may find relaxation times conducting excitation with constant amplitude followed by different pauses.

The extracted data shall be exported a log file.